Efficient and accurate detection of viral sequences at single-cell resolution reveals novel viruses perturbing host gene expression

Laura Luebbert[1], Delaney K. Sullivan[1,2], Maria Carilli[1], Kristján Eldjárn Hjörleifsson[3], Alexander Viloria Winnett[1,2], Tara Chari[1], Lior Pachter[1,3]

[1] Division of Biology and Biological Engineering, California Institute of Technology, Pasadena, California

[2] UCLA-Caltech Medical Scientist Training Program, David Geffen School of Medicine, University of California, Los Angeles

[3] Department of Computing and Mathematical Sciences, California Institute of Technology, Pasadena, California

Abstract

More than 300,000 mammalian virus species are estimated to cause disease in humans. They inhabit human tissues such as the lungs, blood, and brain and often remain undetected. Efficient and accurate detection of viral infection is vital to understanding its impact on human health and to make accurate predictions to limit adverse effects, such as future epidemics. The increasing use of high-throughput sequencing methods in research, agriculture, and healthcare provides an opportunity for the cost-effective surveillance of viral diversity and investigation of virus-disease correlation. However, existing methods for identifying viruses in sequencing data rely on and are limited to reference genomes or cannot retain single-cell resolution through cell barcode tracking. We introduce a method that accurately and rapidly detects viral sequences in bulk and single-cell transcriptomics data based on highly conserved amino acid domains, which enables the detection of RNA viruses covering up to 10^{12} virus species. The analysis of viral presence and host gene expression in parallel at single-cell resolution allows for the characterization of host viromes and the identification of viral tropism and host responses. We applied our method to identify novel viruses in rhesus macaque PBMC data that display cell type specificity and whose presence correlates with altered host gene expression.

Introduction

There are an estimated 10^{31} virions on Earth, which amounts to 10 million virions for every star in the known universe[1,2]. Viruses inhabit oceans, forests, deserts, and human tissues such as the lungs, blood, and brain. More than 300,000 virus species are estimated to cause human disease[3]. However, only 261 species have been detected in humans[4]. Many of these have been implicated in complex diseases such as heart disease and cancer. Recent studies suggest that viruses also play a major, unexpected role in common neurodegenerative disorders such as Alzheimer's, Parkinson's, and multiple sclerosis[5–7]. Accurate detection of viral infections is crucial to understanding viral impact on human health.

Of the 261 known disease-causing viruses, 206 fall into the realm of Riboviria[4], which includes all RNA-dependent RNA polymerase (RdRp)-encoding RNA viruses and RNA-dependent DNA polymerase (RdDp)-encoding retroviruses. Amongst many others, these include Corona-, Dengue, Ebola-, Hepatitis B, influenza, Measles, Mumps, Polio-, West Nile, and Zika viruses. Existing workflows for detecting viruses in transcriptomics data rely on the availability of pre-assembled reference genomes. Currently, NCBI RefSeq hosts 5,970 Riboviria reference genomes — a diminutive fraction of Riboviria viruses. Pioneering work by Edgar *et al.*[8] leveraged a well-conserved amino acid sub-sequence of the RdRP, called the 'palmprint', to identify RNA viruses in 5.7 million globally and ecologically diverse sequencing samples from the Sequence Read Archive (SRA)[9]. Their method's independence from pre-computed indices

```
# 1. Install kb-python (optional: install gget to fetch the host genome and/or transcriptome)
pip install kb-python gget

# 2. Create reference index
# Optional: masking of host genomic and/or transcriptomic sequences using the D-list
# Single-thread runtime: 1.5 h; Max RAM: 4.4 GB; Size of generated index: 593 MB
# Without D-list: Single-thread runtime: 3.5 min; Max RAM: 3.9 GB; Size of generated index: 592 MB
kb ref \
    --aa \
    --d-list $(gget ref --ftp -w dna homo_sapiens) \
    -i index.idx --workflow custom \
    palmdb_rdrp_seqs.fa

# 3. Align sequencing reads and generate count matrix
# Single-thread runtime: 1.5 min per 1 million sequences; Max RAM: 2.1 GB
kb count \
    --aa \
    -i index.idx -g palmdb_clustered_t2g.txt \
    --parity single \
    -x default \
    user_data.fastq.gz
```

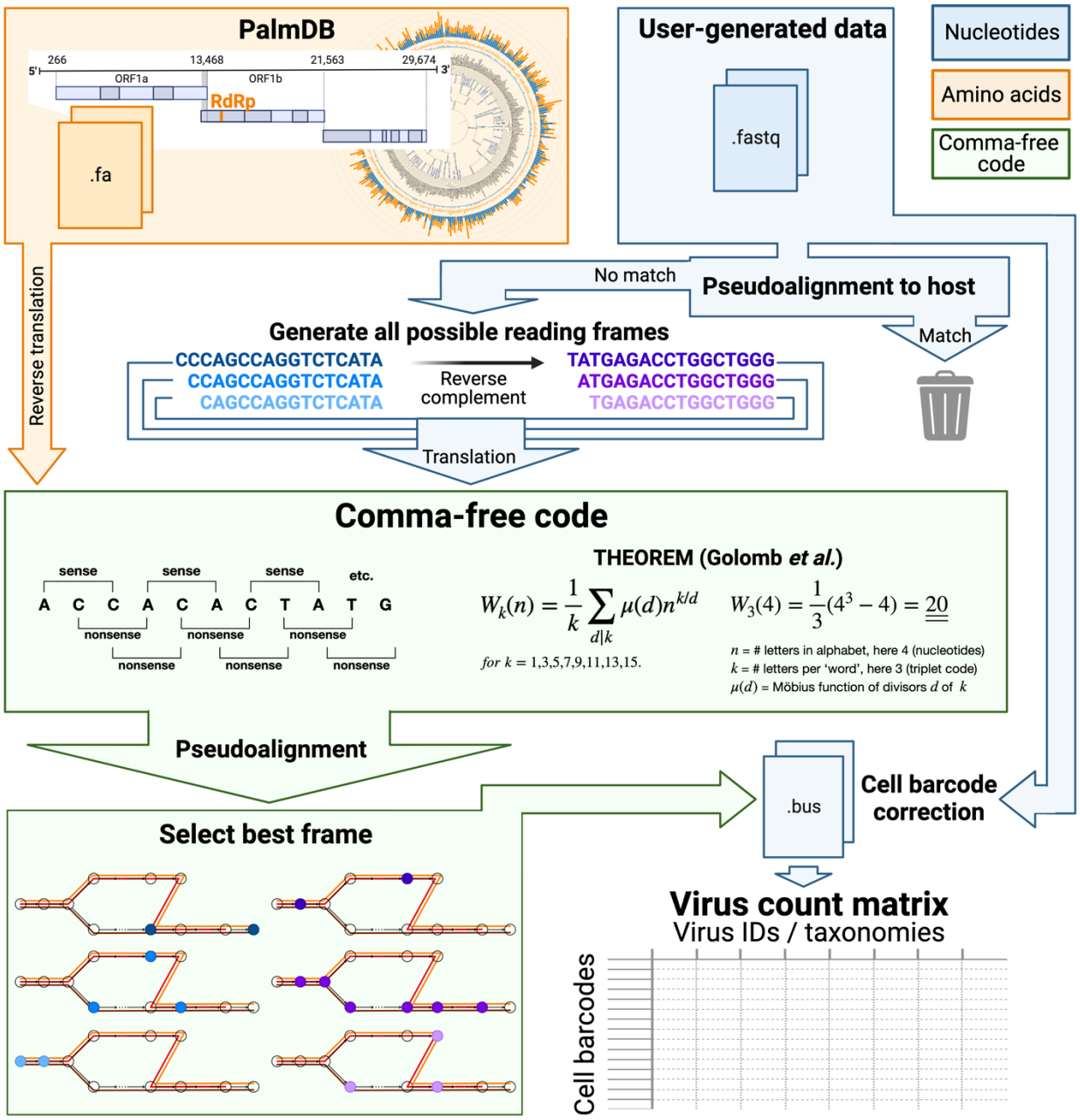

Fig. 1: *Schematic overview of the kallisto translated search front- and back-end. The front-end is similar to kallisto-bustools workflows as previously described[43,44]. The user provides sequencing data, usually in the form of FASTQ files, as well as a reference FASTA file containing amino acid sequences to align the nucleotide sequencing data against. The novel argument '--aa' activates the translated search alignment. In the example shown here, the reference file consists of the PalmDB amino acid RdRP sequences contained in 'palmdb_rdrp_seqs.fa'. The 'palmdb_clustered_t2g.txt' file groups virus IDs with the same taxonomy across all main taxonomic ranks like transcripts of the same gene (see Methods). Both files are available here: https://tinyurl.com/4wd33rey. During the generation of the reference index with 'kb ref', the D-list option may be used to mask host genomic and/or transcriptomic sequences, as further discussed in this manuscript. Here, human genomic sequences fetched from Ensembl using gget[45] are masked using the D-list. The reference index only needs to be generated once, and precomputed PalmDB reference indices for human and mouse hosts are available here: https://tinyurl.com/aaxyy8v8. Following the generation of a reference index, the sequencing reads are pseudoaligned to the reference index, and a count matrix is generated using the 'kb count' command. The '-x' argument is used to define the sequencing technology. In the example code, the minimum required user input is marked in orange (amino acid space) and blue (nucleotide space). In the kallisto translated search back-end, the reference amino acid sequences and the nucleotide sequencing reads are translated into a non-redundant comma-free code. For the nucleotide sequences, the translation occurs in all six possible reading frames (three forward and three reverse frames). The pseudoalignment is performed in the comma-free code space and is compatible with the kallisto cell barcode tracking which enables analysis at single-cell resolution. The workflow generates a cell barcode by virus ID count matrix.*

allowed alignment to diverged sequences, leading to the discovery of thousands of novel viruses. This effort resulted in a consensus of 296,623 unique RdRP-containing amino acid sequences, henceforth referred to as 'PalmDB', representing an estimated 10^8 to 10^{12} virus species[8]. While the RdRP is highly conserved across Riboviria, species-like operational taxonomic units (sOTUs), obtained by clustering the palmprints, serve to approximate taxonomic assignment[8,10] and allow species-level virus identification for 40,392 sequences in the PalmDB.

The increasing use of high-throughput next-generation sequencing (NGS) methods in molecular biology research, agriculture, and healthcare provides an opportunity for the cost-effective surveillance of viral diversity and the investigation of virus-disease correlations[11,12]. Specifically, single-cell genomics technologies make possible, in principle, the characterization of viruses at single-cell resolution. We expanded the RNA sequencing data preprocessing tool kallisto[13] to support the detection of viral RNA using the amino acid database PalmDB. To our knowledge, this is the only existing method capable of translated alignment while retaining single-cell resolution. The small size of PalmDB (36 MB) enables efficient detection of orders of magnitude more viruses than detection based on (NCBI) reference genomes. Moreover, operating in the amino acid space yields a method robust to nucleotide point mutations.

Results

Translated alignment of nucleotide sequences to an amino acid reference with kallisto enables efficient, accurate detection of up to 10^{12} RNA viruses in transcriptomic data at single-cell resolution

Existing methods to detect viral sequences either (i) rely on and are limited to (NCBI) reference genomes[14–23], (ii) are not able to perform translated alignment of nucleotide data to an amino acid reference[24–26], or (iii) are unable to retain single-cell resolution through cell barcode tracking[27,28] (Fig. 2b). We expanded the bulk

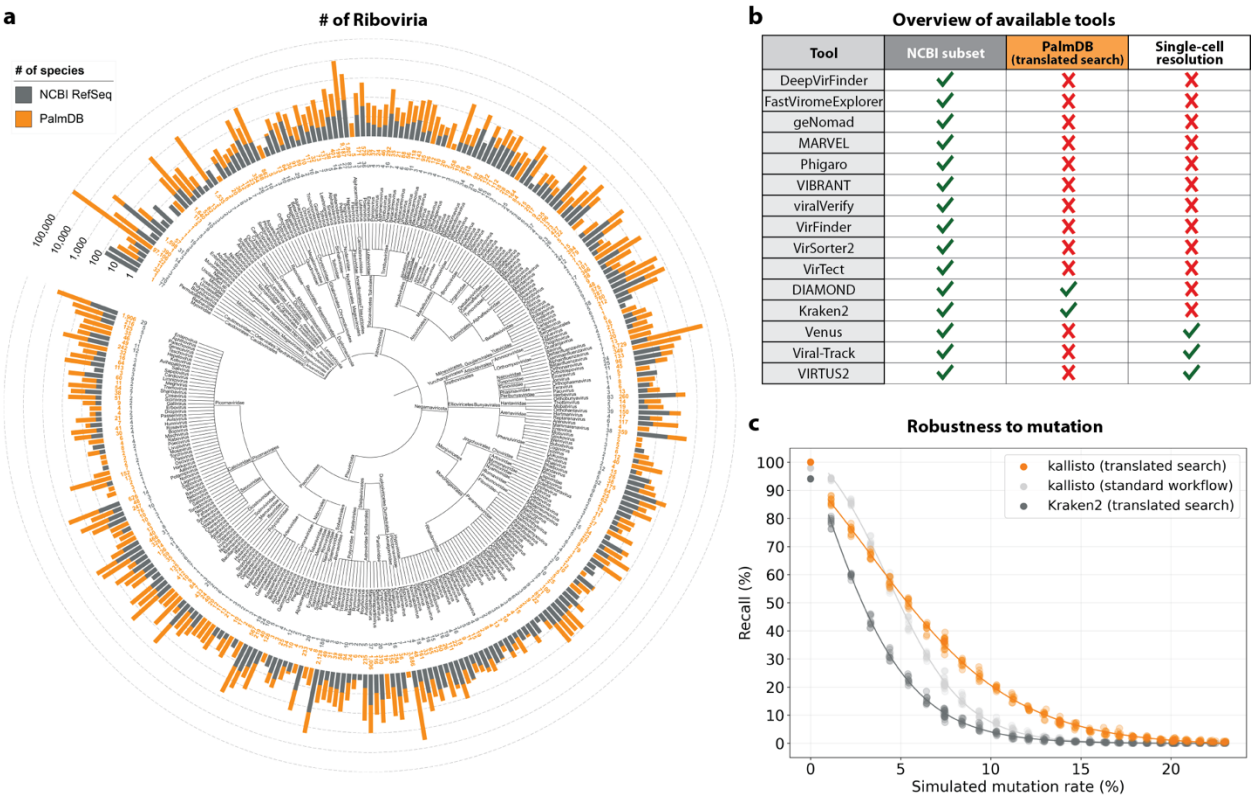

Tool	NCBI subset	PalmDB (translated search)	Single-cell resolution
DeepVirFinder	✓	✗	✗
FastViromeExplorer	✓	✗	✗
geNomad	✓	✗	✗
MARVEL	✓	✗	✗
Phigaro	✓	✗	✗
VIBRANT	✓	✗	✗
viralVerify	✓	✗	✗
VirFinder	✓	✗	✗
VirSorter2	✓	✗	✗
VirTect	✓	✗	✗
DIAMOND	✓	✓	✗
Kraken2	✓	✓	✗
Venus	✓	✗	✓
Viral-Track	✓	✗	✓
VIRTUS2	✓	✗	✓

Fig. 2: ***a****, Phylogenetic tree of the taxonomies of viral sequences/genomes included in the PalmDB and NCBI RefSeq databases from phylum to genus. Barplots indicate the number of sequences/species available for each taxonomy in each database. The tree was generated with iTOL*[46]*. This plot can also be viewed interactively here: tinyurl.com/4dzwz5ny.* ***b****, Overview of available tools for the detection of viral sequences in next-generation sequencing data*[14–26,28,47]*, and their ability to align to NCBI RefSeq nucleotide genomes, perform translated alignment of nucleotide data against an amino acid reference, and retain single-cell resolution through cell barcode tracking.* ***c****, Mutation-Simulator*[48] *was used to add random single nucleotide base substitutions to 676* ZEBOV *RdRP sequences obtained by Seq-Well sequencing*[37] *at increasing mutation rates. We performed 10 simulations per mutation rate. The sequences were subsequently aligned using kallisto translated search against the complete PalmDB, Kraken2 translated search against the RdRP amino acid sequence of* ZEBOV *with a manually adjusted NCBI Taxonomy ID to allow compatibility with Kraken2, and kallisto standard workflow against the complete* ZEBOV *nucleotide genome (GCA_000848505.1). The plot shows the recall percentage of the 676 sequences for each of the 10 simulations at each mutation rate. Each was fitted with an inverse sigmoid for mutation rates > 0.*

and single-cell RNA-seq preprocessing tool kallisto[13] to allow translated search and validated its use in combination with PalmDB for the detection of viral sequences in single-cell and bulk RNA sequencing data. PalmDB is a database of 296,623 unique RdRP-containing amino acid sequences, representing an estimated 10^8 to 10^{12} virus species.[8] Compared to the 5,970 Riboviria reference genomes currently available on NCBI, this signifies a more than 16,000x increase in the number of viruses that can be detected. Fig. 2a provides an overview of the number of entries per taxonomy in NCBI and PalmDB. The figure can also be viewed interactively here: tinyurl.com/4dzwz5ny.

The translated alignment is performed by first reverse translating the amino acid reference sequences and all possible reading frames (three forward and three reverse) of the nucleotide sequencing reads to comma-free code (Fig. 1)[29]. A comma-free code is a set of k-letter 'words' selected such that any off-frame k-mers formed by adjacent letters do not constitute a 'word', and will thus be interpreted as 'nonsense'. For k=3 (a triplet code) and 4 letters (e.g. 'A', 'T', 'C', and 'G'), this results in exactly 20 possible words (theorem shown in Fig. 1), which equals the number of amino acids specified by the universal genetic code. Due to the serendipity of these numbers, Crick *et al.* hypothesized the genetic code to be a comma-free code in 1957[30]. The impossibility of off-frame matches makes comma-free codes highly appropriate for translated alignment (Extended Data Fig. 10, Methods). The *de Bruijn* graph generated from the reverse translated PalmDB sequences groups viruses of the same taxonomies, indicating that within-taxonomy similarity is conserved in comma-free space as expected (Extended Data Fig. 4d). Finally, the six reading frames of the sequencing reads translated to comma-free code are pseudoaligned to the reference sequences reverse translated to comma-free code. If several reading frames of the same read produce alignments, the best frame is chosen (Fig. 1).

The workflow can be executed in three lines of code, and computational requirements do not exceed those of a standard laptop (Fig. 1). Building on kallisto's versatility, the workflow is compatible with all state-of-the-art single-cell and bulk RNA sequencing methods, including but not limited to 10x Genomics, Drop-Seq[31], SMART-Seq[32], SPLiT-Seq[33] (including Parse Biosciences), and spatial methods such as Visium.

Validation testing was performed using different bulk and single-cell RNA sequencing datasets with known infections with severe acute respiratory syndrome coronavirus 2 (SARS-CoV-2) or *Zaire ebolavirus* (ZEBOV)[34–38]. In these tests, translated search with kallisto and PalmDB was able to detect the viral RNA and correctly assign species-level taxonomy at counts correlating with viral loads measured by RT-qPCR or RNA-ISH, regardless of the technology used to generate the data (Fig. 3a). Fig. 3b provides an overview of the accuracy of the taxonomic assignment across all available taxonomic ranks after reverse translated RdRP sequences were aligned to the PalmDB with kallisto translated search. At the species level, 96.76 % of 296,561 sequences were assigned the correct taxonomy, 0.007 % were assigned an incorrect taxonomy, 0.37 % could not be unambiguously matched to a single virus (they were multimapped), and 2.86 % were not aligned.

Next, we sought to confirm that kallisto translated search with PalmDB correctly identifies sequences that originate from the RdRP gene. To this end, we selected a subset of 100,000,000 reads obtained using Seq-Well sequencing of macaque peripheral blood mononuclear cell (PBMC) samples obtained at 8 days post-infection with ZEBOV[37] (see Methods). We aligned the reads to the PalmDB amino acid sequences with kallisto translated search. We also aligned the reads to the complete ZEBOV nucleotide genome using Kraken2 (standard nucleotide alignment)[27]. Aligned reads from both alignments were extracted and realigned to the ZEBOV genome using bowtie2[39], a BAM file was created using SAMtools[40] and the alignment was subsequently visualized NCBI Genome Workbench[41]. The visualized alignments are shown in Extended Data Fig. 2 and confirmed that kallisto translated search accurately and comprehensively detected ZEBOV RdRP sequences.

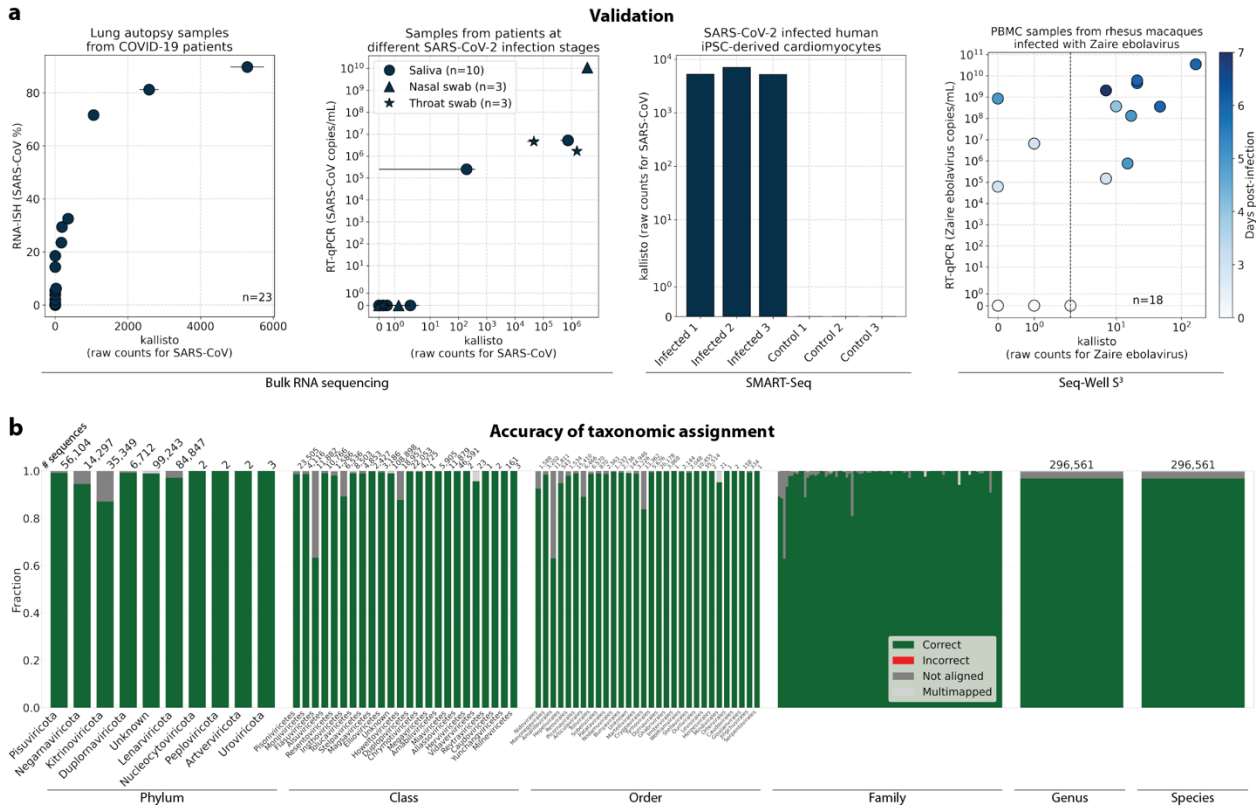

***Fig. 3: a**, Sequencing data from samples with a known viral infection and sequenced using different bulk and single-cell RNA sequencing technologies was aligned to PalmDB using kallisto translated search. Viral load obtained through alternative methods, such as RNA-ISH and qPCR, is compared to the target virus counts returned by kallisto. From left to right: 1. RNA-ISH (%) over total raw kallisto counts for SARS-CoV for 23 lung autopsy samples from COVID-19 patients obtained by bulk RNA sequencing[34]. Error bars show min-max values for each read in a pair; the dot shows the mean. 2. SARS-CoV-2 viral load by RT-qPCR (copies/mL) over total raw kallisto counts for SARS-CoV species obtained by bulk RNA sequencing of 16 saliva (circle), nasal swab (triangle), and throat swab (star) specimens from patients with acute SARS-CoV-2 infection[35,36]. Each specimen underwent duplicate library preparation and paired-end sequencing; points indicate the mean among the paired reads and duplicates, and error bars show min-max values. 3. Total raw kallisto counts for SARS-CoV species for 3 human iPSC-derived cardiomyocytes infected with SARS-CoV-2 and 3 control samples obtained by SMART-Seq[38]. 4. RT-qPCR (copies/mL) over total raw kallisto counts for* ZEBOV *for 19 rhesus macaque blood samples obtained during different stages of infection with* ZEBOV *and sequenced with Seq-Well[37]. **b**, To validate the mapping of nucleotide sequences to an amino acid reference with kallisto translated search and assess the accuracy of the taxonomic assignment, we reverse translated all amino acid sequences in the PalmDB using the 'standard' genetic code (see Methods). The reverse translated PalmDB RdRP sequences were subsequently aligned to the optimized PalmDB amino acid reference (see Methods) with kallisto translated search. For each sequence, we differentiated the mapping result at each taxonomic rank into four categories: 'correct' or 'incorrect' taxonomic assignment based on the sOTU to virus ID mapping, 'multimapped' (the sequence aligned to multiple targets in the reference and could not unambiguously be assigned to one), or 'not aligned' (the sequence was not aligned). The plot shows the fraction of sequences falling into each mapping result category assessed at each taxonomic rank. The numbers above the bars indicate the total number of sequences per rank. Family names and numbers were omitted, and genera and species ranks were combined for readability.*

We then tested whether our translated search method is robust to single nucleotide mutations, which occur at a relatively high rate in RNA viruses of up to 10^{-4} substitutions per nucleotide site per cell infection[42]. We added random single nucleotide base substitutions to 676 ZEBOV nucleotide RdRP sequences identified during the alignment described in the previous paragraph[37], then assessed the frequency of correct taxonomic classification (recall percentage) by kallisto translated search, in comparison to the current state-of-the-art translated search tool, Kraken2 (translated search). kallisto translated search correctly recalled up to 27.5 % more viral RdRP sequences than Kraken2 (translated search) (Fig. 2c). Moreover, kallisto translated search was more robust than aligning to the complete nucleotide genome with the standard kallisto workflow at mutation rates > 4 % (Fig. 2c), which emphasizes the advantage of operating in the amino acid space. While the Kraken2 (translated search) and the kallisto standard workflow were given only the correct virus as a reference (here, ZEBOV), kallisto translated search had to distinguish between all viruses contained in the PalmDB and identify the correct taxonomy. kallisto translated search was able to maintain > 90 % precision in the species-level taxonomic assignment at mutation rates up to 12 % (Extended Data Fig. 4b).

We next sought to investigate whether viral species not included as species-like operational taxonomic units (sOTUs) in the reference PalmDB database could be detected based on the conservation of the RdRP gene. To do this, we removed all Ebola virus species, all *Ebolavirus* genera, and all members of the *Filoviridae* family from the reference, and subsequently aligned the 676 ZEBOV RdRP sequences obtained by Seq-Well sequencing[37]. In each scenario, a subset of sequences aligned to the nearest remaining relative based on the main taxonomic rank (Extended Data Fig. 1). This suggests that kallisto translated search can detect the highly conserved RdRP of a large number of viral species, beyond the number of sequences in the PalmDB database, while still providing reliable sOTU-based taxonomic assignment of lower-rank taxonomies.

Read and virus filtering

A common problem that arises during the identification of microbial sequences is the cross-species contamination of reference genome databases, such as the ubiquitous contamination of bacterial genomes with human DNA[49–51]. This can lead to the misclassification of host reads as bacterial or viral, suggesting the presence of microbes that were not truly present. The misclassification of host reads as viral can be prevented by removing host reads prior to the alignment to the viral reference. However, conservatively removing host reads will also remove sequences of endogenous viral elements, which are very abundant in vertebrate genomes[52] and may lead to the removal of viral sequences that were truly present. Hence, there are two goals: (i) removing host reads to prevent the misclassification of host reads as viral while (ii) comprehensively identifying the virome within a sample.

We first evaluated the impact of different host masking options on the resulting virome. We used kallisto translated search with PalmDB to map the virus profiles of peripheral blood mononuclear cell (PBMC) RNA sequencing samples from 19 rhesus macaques and applied different host masking workflows. The approach to masking host versus microbe reads and the handling of overlap between reference sequences can affect the downstream result. For example, sequences with varying sizes of virus-host overlap, sequences that span the junction of two exons, and entirely ambiguous sequences can influence the outcome of the masking and generate highly variable results depending on the method used (Extended Data Fig. 4a and 5). Depending on the research question and design, any one or a combination of different masking

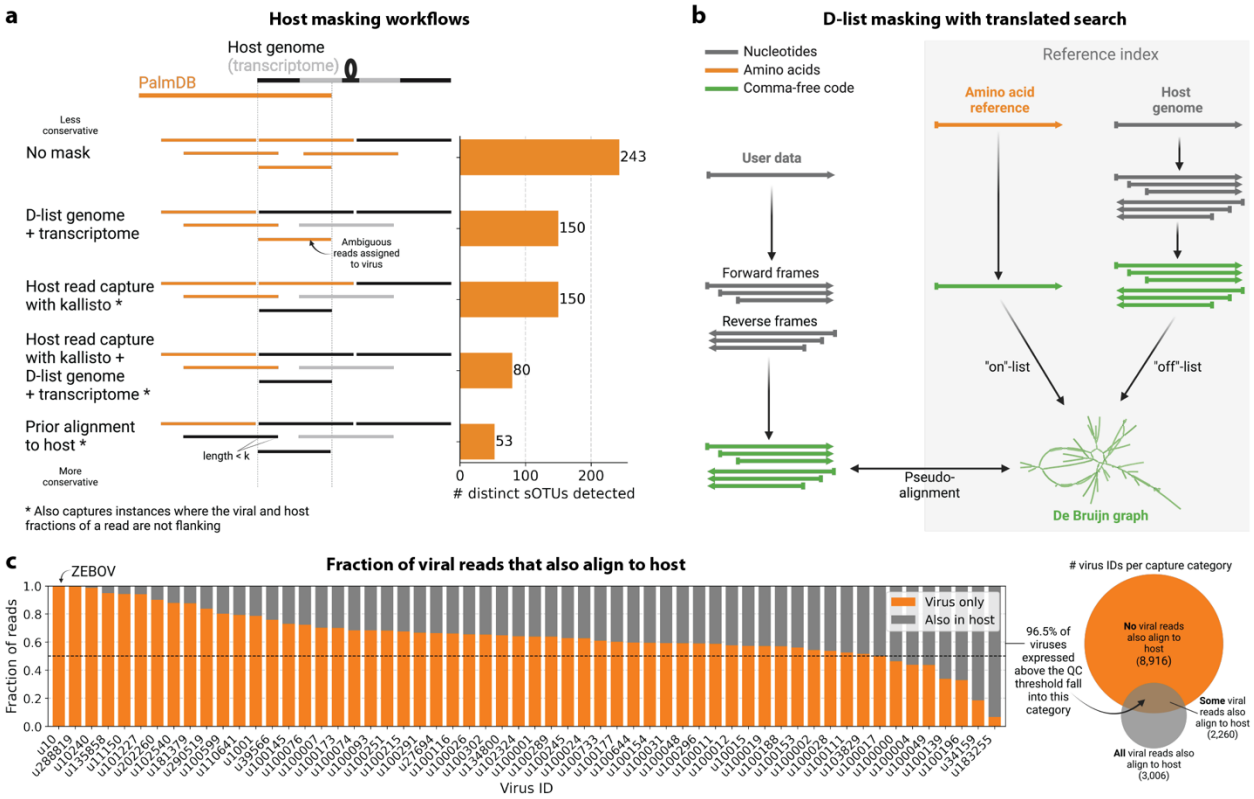

Fig. 4: ***a****, Schematic overview of the different host masking options discussed in this manuscript. Reads that align to PalmDB and are considered viral are marked in orange and reads that align to the host genome or transcriptome are marked in black or grey, respectively. The barplot shows the number of distinct sOTUs, defined by distinct virus IDs observed in ≥ 0.05 % of cells for each workflow.* ***b****, Schematic overview of masking the host genome with the D-list argument when used in combination with translated search. The D-list genome consists of nucleotide sequences and hence is translated to comma-free code in all six possible reading frames, similar to the translation of the nucleotide sequencing reads.* ***c****, Masking host sequences with the kallisto read capture workflow generates two distinct virus count matrices: The first contains viral reads that only aligned to the PalmDB, and the second contains viral reads that aligned to the host transcriptome in addition to the PalmDB. The majority of viruses detected above the quality control (QC) threshold (observed in ≥ 0.05 % of cells), had reads that aligned to the host transcriptome as well as the PalmDB. The barplot shows the fraction of reads for each virus that aligned to the PalmDB only ('virus only') and those that aligned to the host transcriptome in addition to the PalmDB ('also in host').*

options might be appropriate. We explored the following masking options, listed from least to most conservative:

No mask

We aligned the sequencing reads to the PalmDB with kallisto translated search without masking or previously removing host sequences. For the macaque PBMC dataset, this masking option resulted in 243 distinct sOTUs detected (Fig. 4a).

D-list genome + transcriptome

To incorporate host read masking into our kallisto workflow, we quantified the reads while masking the host genome and transcriptome using an index created with the D-list (distinguishing list) option[53]. This option identifies sequences that are shared between a target transcriptome and a secondary genome and/or transcriptome. *k*-mers flanking the shared sequence on either end in the secondary genome are added to the index *de Bruijn* graph. During pseudoalignment, the flanking *k*-mers are used to identify reads that originated from the secondary genome but would otherwise be erroneously attributed to the target transcriptome due to the spurious alignment to the shared sequences. In our experiments, the target transcriptome consisted of the viral RdRP amino acid sequences contained in the PalmDB, and the secondary genome consisted of transcriptomic and genomic macaque and dog nucleotide sequences. When combining D-list with translated search, the secondary genome is translated to comma-free code in all six possible reading frames (Fig. 4b). This masking option can be easily added to the kallisto translated search workflow without any additional commands (Fig. 1). Masking the host transcriptome and genome with D-list resulted in 150 distinct sOTUs detected (Fig. 4a). Note that masking both the transcriptome and the genome, or either one will generate different results because masking only the genome will not mask sequences that span exon-exon junctions (Extended Data Fig. 4a and 5).

Host read capture with kallisto

To imitate prior alignment to the host genome, as performed with bwa (described below), within a simple, efficient kallisto workflow, we captured all reads that pseudoaligned to the host transcriptome with kallisto. Masking by capturing these host reads resulted in the same number of distinct sOTUs detected as masking with D-list (Fig. 4a).

Host read capture with kallisto + D-list genome + transcriptome

Although masking with D-list and capturing reads that aligned to the host transcriptome resulted in the same number of distinct sOTUs detected, the two methods masked different reads and resulted in different virus profiles (Fig. 5a, Extended Data Fig. 5). We decided to combine the D-list and host read capture masking approaches to achieve a conservative result similar to that achieved by prior alignment with bwa. In this approach, the sequencing reads were aligned to the PalmDB index with a D-list containing the host genome and transcriptome, and subsequently reads that pseudoaligned to the host transcriptome were captured. Combining the D-list and host read capture masking options reduced the number of detected sOTUs to 80 (Fig. 4a).

Prior alignment to host with bwa

We aligned the sequencing reads to the macaque and dog genomes using the highly sensitive alignment algorithm bwa[54] and removed all reads that aligned anywhere in the host genomes before alignment to PalmDB with kallisto translated search. This achieved very conservative masking of the host genome. However, this workflow is complex, time-consuming, and computationally expensive (~4.5 days using 60 cores for the macaque ZEBOV PBMC dataset). This workflow resulted in the detection of 53 distinct sOTUs (Fig. 4a).

There are inherent differences between these masking methods which are illustrated in Fig 4a and Extended Data Fig. 4a. Although the genome is passed to the software, the standard kallisto workflow builds an index based on the host transcriptome, not the entire host genome, since for genomes as large as the macaque genome, building the index on the entire genome would require a large amount of memory. Hence, masking

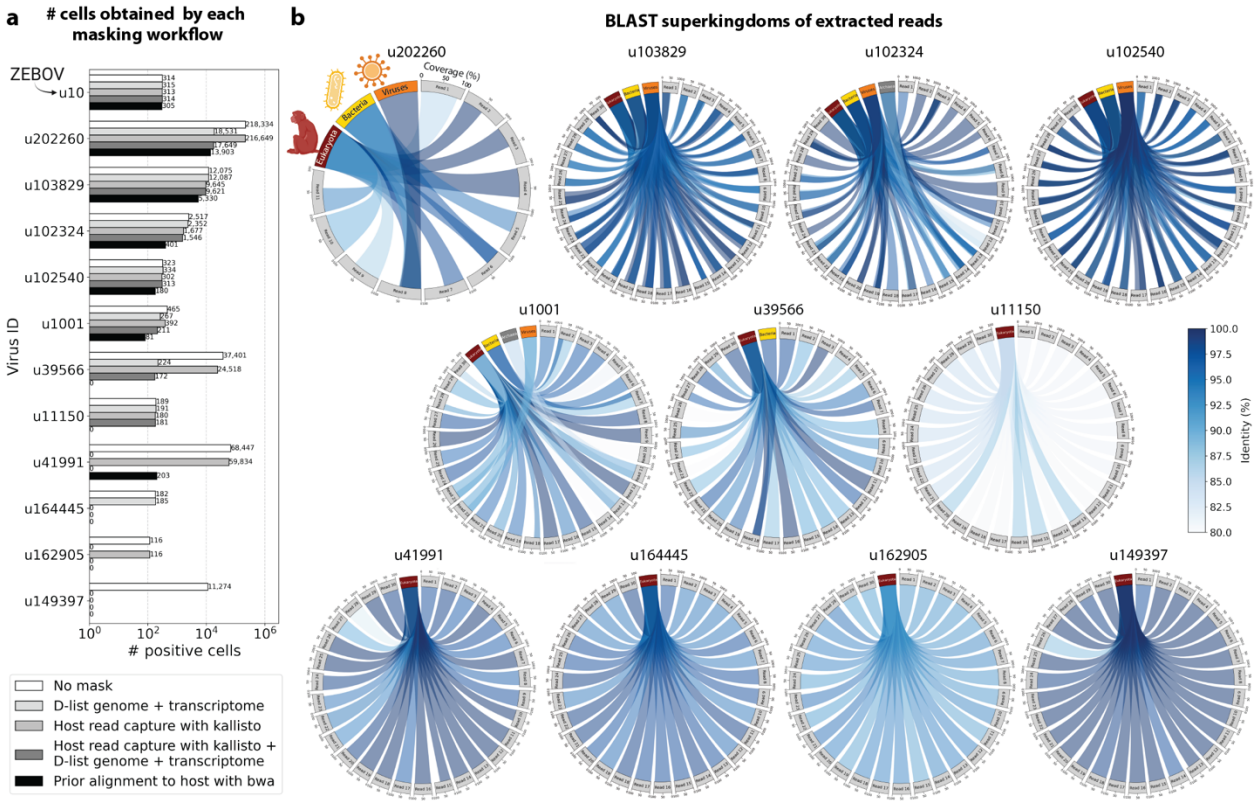

Fig. 5: ***a****, The number of positive cells obtained for 12 different virus IDs by each masking workflow. Each masking workflow is described in detail in the Methods section. The cell counts for all viruses detected above the QC threshold for all masking workflows are shown in Extended Data Fig. 5.* ***b****, pyCirclize plots showing the BLAST+[55,56] results of randomly selected sequencing reads for each of the novel viruses shown in a (excluding the known virus ZEBOV which corresponds to virus ID 'u10'). Each circular plot corresponds to the results for one virus ID. Each light grey sector corresponds to one sequencing read that links to the superkingdoms (red (eukaryotes), yellow (bacteria), orange (viruses), and dark grey (archaea) sectors) based on its BLAST+ alignment results. The width of the connecting link indicates the BLAST+ alignment coverage percentage, and its color indicates the identity percentage. For u202260, approximately ⅔ of the extracted reads yielded no BLAST results.*

by capturing reads that pseudoaligned to the host with kallisto will only capture host reads from mature mRNA molecules. If the D-list is passed both the transcriptome and the genome, it will be able to mask mature and nascent RNA molecules as well as RNA molecules originating from intergenic regions. The D-list index avoids excessive memory requirements by restraining the index to distinguishing sequences between viral and host sequences. As a result, reads that contain non-flanking host and viral sequences will not be filtered. Moreover, the D-list will favor viral assignment in the case of an entirely ambiguous read. Neither of these issues applies to masking with bwa, since the alignment with bwa was performed against the host genome. Since bwa uses a smaller seed length than kallisto's default k-mer size of 31, bwa provides more sensitive alignment of sequencing reads against the host genome and provides the most stringent filtering.

To confirm that reads identified as viral were not misaligned macaque reads, we extracted randomly selected sequencing reads from 11 virus IDs and aligned them against the nucleotide sequence database

with BLAST+[55,56] (Fig. 5b). The reads associated with virus IDs identified by all masking workflows (u202260, u103829, u102324, u102540, and u1001) BLAST-aligned with relatively low coverage and identity to several superkingdoms, including viruses. For u202260, approximately ⅔ of the extracted reads yielded no BLAST results. Given that the majority of RdRP sequences in the PalmDB originate from unknown viruses lacking reference genomes, it was expected that these sequences would not yield confident BLAST results. However, given the comprehensiveness of the macaque genome[57], misaligned macaque sequences should BLAST to the macaque genome with high coverage and identity. The next two virus IDs, u39566 and u1150, were filtered out by the bwa workflow and did not BLAST to the viruses superkingdom. However, their BLAST results displayed relatively low coverage and identity, which would not be expected from macaque sequences. Below, we provide further evidence that u1150 sequences might have originated from an ongoing viral infection. This was likely an instance where filtering with bwa was too conservative and threw out viral sequences. u41991 was identified as viral by the bwa workflow but filtered out by the D-list + host capture workflow. Based on the BLAST results for u41991, which include high coverage and identity matches for eukaryotes, it is likely that filtering is the appropriate action. u164445 and u162905 were filtered by either capturing the host reads or using the D-list, respectively, and BLAST to eukaryotes with high coverage and identity, illustrating that a combination of the two methods leads to more robust results. Finally, sequences identified as u149397, which were filtered by all masking options and are only retained without masking, BLAST to eukaryotes with high coverage and identity.

Separately from exploring the results of different read masking options, we also investigated the question of virus filtering. Host read capture with kallisto generates two separate count matrices: One contains counts for reads that are solely viral, and a second contains counts for viral reads that also pseudoaligned to the host transcriptome. The distinction between filtering reads and filtering viruses becomes evident when examining the two count matrices: for the macaque PBMC dataset, we found that most viruses found in ≥ 0.05 % of cells had at least some reads that also mapped to the host transcriptome, including 2 reads for ZEBOV (Fig. 4c). Moreover, aligning without host masking often led to the detection of more positive cells (Extended Data Fig. 5). Hence, naive masking of reads can lower the detection sensitivity of viruses that seem truly present. Our masking workflows facilitate the identification of viruses with a high likelihood of being truly present based on conservative host read masking, while also obtaining unmasked reads for these viruses to prevent the decrease in sensitivity inherent to masking host reads. We applied this approach when training the logistic regression models described below to minimize the occurrence of false viral absence.

The presence of novel viruses perturbs host gene expression in macaque blood cells, allowing prediction of viral presence based on host gene expression at single-cell resolution

We used kallisto translated search and the PalmDB to map the viral profiles of PBMC samples from 19 rhesus macaques sequenced at different stages of Ebola virus disease (EVD)[37] (Fig. 6a) at single-cell resolution. The dataset consisted of 30,594,130,037 reads in total. After alignment to both the host genome (using the standard kallisto workflow) and PalmDB (using kallisto translated search with D-list + host capture masking), and quality control using the host count matrix (Extended Data Fig. 3a, Methods), we retained 202,525 PBMCs. We used the Leiden algorithm[58] to partition the PBMC transcriptomes into 18 clusters of similar macaque gene expression, of which 16 could be assigned cell types based on common marker genes (Extended Data Fig. 3d).

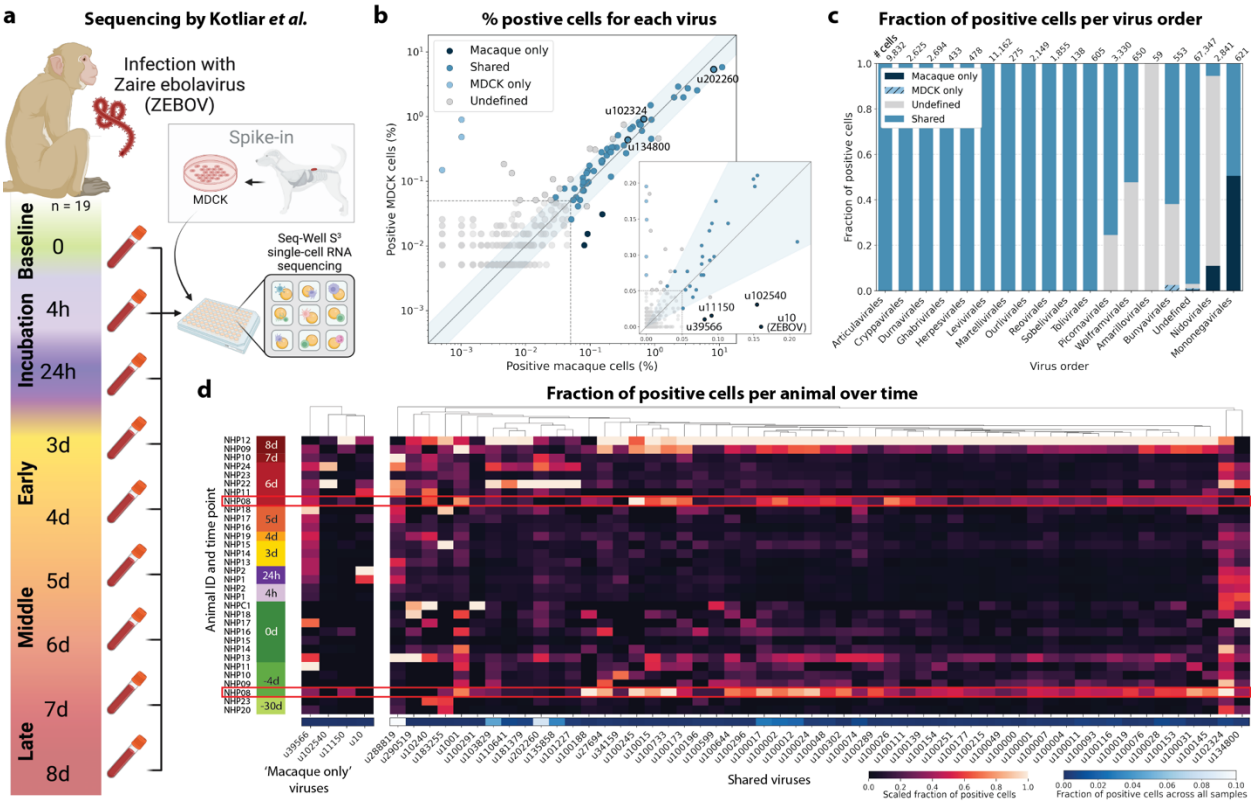

Fig. 6: ***a****, Schematic overview of the single-cell RNA sequencing data collected by Kotliar et al.[37]. Kotliar et al. performed single-cell RNA sequencing of peripheral blood mononuclear cell (PBMC) samples from 19 rhesus macaques at different time points during Ebola virus disease (EVD) after infection with Zaire Ebolavirus (ZEBOV) using Seq-Well[82] with the S3 protocol[83]. A subset of the PBMC samples were spiked with Madin-Darby canine kidney (MDCK) cells. This schematic was adapted from the original design by Kotliar et al.* ***b****, For each virus, the percentage of positive MDCK cells is plotted against the percentage of positive macaque cells. The viruses were categorized into 'shared', 'macaque only', 'MDCK only', and 'undefined' viruses as described in the Methods section. The insert shows the same plot without log scale axes such that zero counts are included.* ***c****, Bar plot showing the fraction of positive cells obtained for each virus order, as defined by the PalmDB sOTUs, for each virus category.* ***d****, Fraction of positive cells for all 'macaque only' and 'shared' viruses. Each row corresponds to one animal at a specific EVD time point. The fractions were scaled to range from zero to one for each virus. The raw total fraction of positive cells for each virus across all samples is shown in blue below.*

The obtained cell types, their marker gene expression and relative abundance over time are consistent with the results reported by Kotliar *et al.*[37], including the emergence of a cluster of immature neutrophils and decreased lymphocyte abundance, especially natural killer cells, during EVD (Fig. 7a). While density based PBMC isolation typically removes neutrophils, immature neutrophils are less dense than mature neutrophils and can co-isolate with PBMCs during infections[37]. Clusters of the same cell type were often separated by time point (Fig. 7a), indicating changes in macaque gene expression within the same cell type over the course of the EVD. This is in agreement with results obtained by mass cytometry in Kotliar *et al.*[37].

ZEBOV count data from this analysis workflow was also consistent with previously reported results. Since only a small fraction of the RNA molecules in these tissue samples are viral and of those we only detect the RdRP, the measured absolute RNA counts for any one virus per cell are low (Extended Data Fig. 3e). As a

result, we converted the virus count matrix into a binary matrix where each virus was recorded as being either present or not present in each cell. This approach has been previously validated for sparse single-cell RNA, specifically viral, sequencing data[24,59], and prevented the need for further normalization by individual cellular viral load, which may introduce biases[49]. The presence of virus in each cell was then used to determine the viral abundance among populations of cells composed of clusters, cell types, or tissues. First, we used the binary virus count matrix to validate the detection of ZEBOV. Samples obtained during incubation displayed the highest abundance of ZEBOV-positive cells, and ZEBOV-positive cells remained detectable at all following time points (Fig. 7b, top left). These trends are consistent with the results reported by Kotliar *et al.*[37].

The parallel analysis of viral and host gene counts at single-cell resolution allowed the identification of infected cell types based on host gene expression to reveal that ZEBOV-positive cells consisted predominantly of monocytes (Fig. 7b, top right). These results are consistent with previous literature on ZEBOV tropism[60] and reproduce the ZEBOV abundance trends obtained by alignment to the ZEBOV genome[37]. This indicates that while the total viral counts obtained by kallisto translated search with PalmDB are low due to only detecting the RdRP, comparative trends are captured accurately. All Ebola virus reads were identified correctly as ZEBOV with no counts detected for other Ebola virus species (Extended Data Fig. 6).

Our analysis workflow identified viruses other than ZEBOV in this dataset. These viruses may be present due to infection of the host, host endogenous viral elements, infection of bacteria residing in the host, infection of food ingested by the host, or laboratory contamination. Fig. 7b (bottom left and right) shows the total number of distinct sOTUs (corresponding to distinct virus IDs) detected over time and per cell type. We observed a slight increase in the number of distinct sOTUs detected per cell during the later stages of EVD, driven by T cell, B cell, and neutrophil clusters with high fractions of cells during later EVD stages (Fig. 7a). Neutrophils showed the highest numbers of distinct viruses per cell (Fig. 7b, bottom right). Since neutrophils fulfill their microbicidal function through phagocytosis and pinocytosis, it is possible that the viral RNA was picked up by these cells through ingestion rather than cellular infection.

Among the samples in this dataset, we detected a total of 11,176 viruses with at least one read that aligned to the PalmDB and did not align to the host (Fig. 4c), including many viruses from genera known to infect rhesus macaques (Extended Data Fig. 6)[61]. However, the majority of these viruses were expressed in less than 0.05 % of cells, which we defined as a quality control (QC) threshold (Fig. 6b, Methods). All of the viruses with positive cell fractions above the QC threshold in macaque cells that passed quality control can be explored in this interactive Krona plot[62] broken down by animal, timepoint, taxonomy, and fraction of cells occupied by each virus: https://tinyurl.com/23h6k36u. A subset of samples included a spike-in of Madin-Darby canine kidney (MDCK) cells, resulting in a total of 23,500 MDCK cells after quality control and species separation (Extended Data Fig. 3b and c, Methods). We used the spike-in to further break down the viruses into "macaque only", "MDCK only", and "shared" viruses (Fig. 6b, Methods). We expected that shared viruses occurring in both macaque and MDCK cells would include viruses introduced by the contamination of laboratory reagents used during sample preparation and sequencing[63], cell-free RNA contamination, endogenous retroviruses[52,64], and widespread latent infections. After filtering and categorization of viruses, we detected 4 (including ZEBOV) macaque only, 7 MDCK only, 15 undefined, and 54 shared viruses. The sOTUs of the macaque only and shared virus IDs, when available, are listed in Extended Data Table 1. Fig. 6c shows the fraction of reads occupied by each viral order for macaque only,

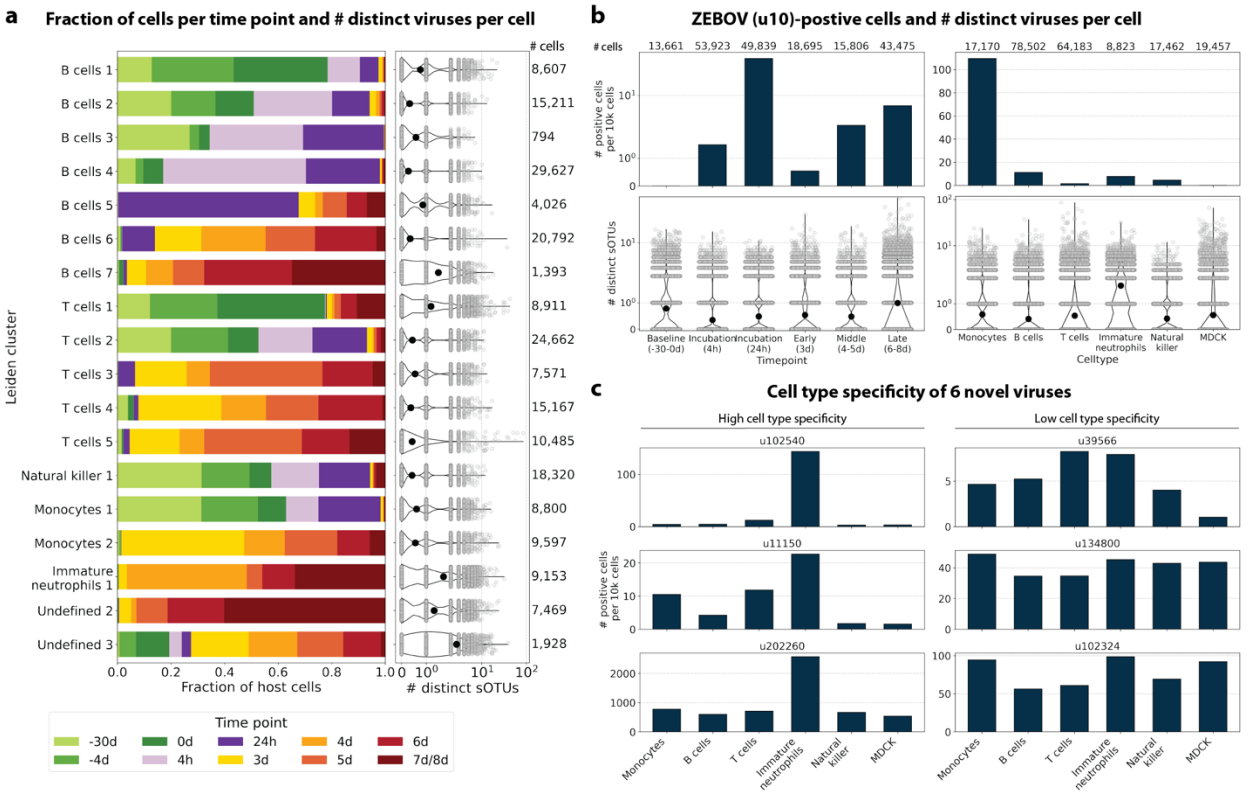

Fig. 7: ***a****, The fraction of cells occupied by each EVD time point is shown per Leiden cluster. Each Leiden cluster was assigned a cell type based on previously defined marker genes (Extended Data Fig. 3d). On the right, the number of distinct viruses, defined by different sOTUs / virus IDs, detected in each cell is shown. Each grey dot corresponds to one cell, and the black dot corresponds to the mean across all cells.* ***b****, The number of ZEBOV (u10) positive cells per 10,000 cells is plotted per EVD time point (left) and per cell type (right). For each time point and cell type, the number of distinct viruses, defined by different sOTUs / virus IDs, found per cell is plotted at the bottom. Each grey dot corresponds to one cell, and the black dot corresponds to the mean across all cells.* ***c****, For 6 novel viruses, the number of positive cells per 10,000 cells is shown per cell type. Virus IDs that show relatively high cell type specificity are shown on the left, and virus IDs with relatively even detection across all cell types are shown on the right.*

MDCK only, and shared viruses. Among viruses shared between macaque and MDCK cells, Levivirales (recently renamed to Norzivirales[65]), Articulavirales (which include the family of influenza viruses), and viruses of unknown taxonomy made up the largest fractions. Norzivirales are an order of bacteriophages, the majority of which were discovered in metagenomics studies[66]. They might have been introduced through bacterial contamination during sample preparation and sequencing. The shared viruses also included orders such as Herpesvirales, which are widespread, sometimes spreading through cross-species infections, and are known to persist in their host as latent infection[67,68]. Viruses infecting MDCK cells included the order of Bunyavirales, which infect a wide range of hosts, including MDCK cells[69], as well as viruses of unknown order. Viruses found only in macaque cells were of unknown order, in the order Mononegavirales, which includes ZEBOV, and in the order Nidovirales, which are known to infect mammals and include the family *Coronaviridae*. Viruses of known order for each group are reasonably

expected to be present in the respective sample types and the context of the hosts, which supports the biological validity of these viral read classifications.

To visualize the virus profiles of individual animals and over time, we plotted the fraction of positive cells for each macaque only and shared virus ID per animal and time point (Fig. 6d). The relative viral abundances varied, both between individual monkeys and time points. Notably, in some instances where the same animal was measured across several time points, the viral profile of this animal was reproduced in the later time point. The viral profiles of animal NHP08 at -4 days pre-infection and 6 days post-infection with ZEBOV are highlighted in the heatmap (Fig. 6d). NHP1 and NHP2 each had two samples sequenced 20 hours apart which displayed highly similar viral profiles for each animal over time (Fig. 8a). This suggests that viral profiles sampled and sequenced within a short time window are coherent over time and across samples which is consistent with expectation. Several viruses, including u102324, were present in all animals and time points with relatively similar abundance (Fig. 6d, Extended Data Fig. 7a).

We then attempted to further determine which viruses were likely present due to infection of the host based on cell-type specificity and a coinciding host antiviral response. We visualized the viral tropism of three viruses that displayed relatively high sample-specificity, u102540, u11150, and u202260, and three viruses that were abundant across all samples, u39566, u134800, and u102324. The sOTU of u102540 indicates that it is an *Alphacoronavirus sp.*, which are known to infect rhesus macaques[61]. u102324 is predicted to belong to the family *Iflaviridae* (Extended Data Table 1), which is a family of viruses that infect insects[70], and the viral reads from this virus ID were likely not the result of an ongoing viral infection. The remaining 4 virus IDs, u11150, u202260, u39566, and u134800, are of unknown taxonomy across all taxonomic ranks. There was little cellular overlap between these viruses, as well as with the known infection with ZEBOV (u10), in the virus count matrix (Extended Data Fig. 7b).

Several viruses exhibited cell-type specificity suggestive of infection. We found that u102540, u11150, and u202260 showed high cell type specificity, while u39566, u134800, and u102324 were expressed more evenly across all cell types (Fig. 7c). u102540 (*Alphacoronavirus sp.*) exhibited high fractions of positive cells in neutrophils, while u11150 and u202260 also displayed lower expression in monocytes, B cells, and T cells. Neutrophils play an important role in the innate immune response and promote virus clearance through phagocytosis. During phagocytosis, neutrophils engulf virions and apoptotic bodies. It is possible that the cell type specificity towards neutrophils observed here was due to neutrophils engulfing viral RNA during phagocytosis rather than viral tropism.

The simultaneous analysis of the host and virus count matrices supported that several viruses identified were likely infecting the host and revealed virus-induced host gene expression. We hypothesized that viral presence in individual cells may be predicted based on the host gene expression. Since our workflow maintains single-cell resolution, we can analyze viral presence and host gene expression at single-cell resolution in parallel, and investigate whether the presence of a virus affects host gene expression. We trained logistic regression models for u102540, u11150, u20226, u39566, u134800, and u102324 to predict viral presence or absence in individual cells based on the cell's host gene expression. The models were either trained on all or only highly variable macaque genes and with or without the covariates donor animal and time point. After training models using a random selection of virus-positive and an equal number of virus-negative cells, we tested the model predictions on held-out test cells (Fig. 8b, Extended Data Fig. 8a). We found that the presence or absence of viruses that displayed cell type- and sample-specificity (u10

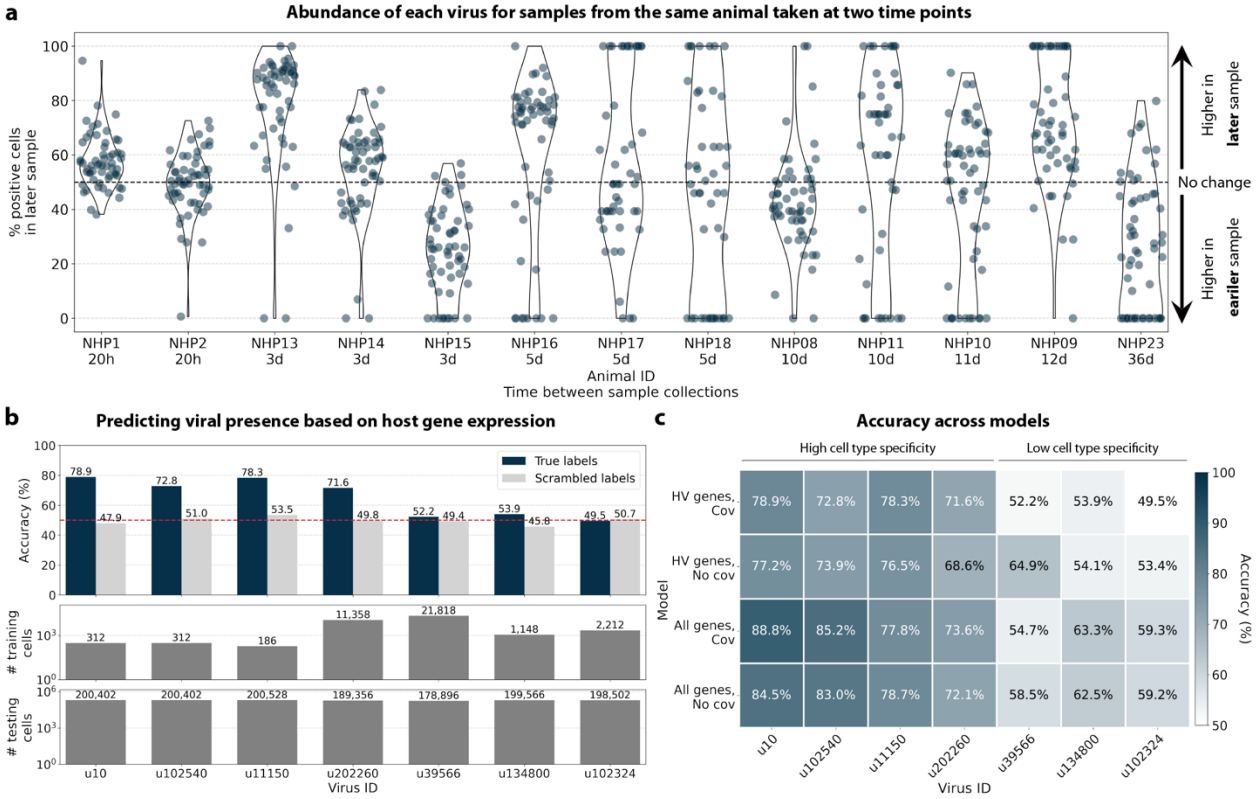

Fig. 8: ***a****, Several animals included in the macaque PBMC dataset were sampled twice, at two different time points. Here, for each virus, the percentage of positive cells occupied by the later time point is shown. The number of positive cells for each virus was first normalized to the total number of cells in the sample. Only viruses for which at least one time point had positive counts were included for each animal. A percentage of 50% indicates that the number of positive cells for that virus remained stable between the two time points.* ***b****, We trained logistic regression models to predict the presence of specific viruses based on host gene expression at single-cell resolution. The accuracy of the logistic regression model trained on highly variable (HV) macaque genes with donor animal and EVD time point as covariates is shown for the known virus ZEBOV (u10) and 6 novel viruses. The presence of viruses that displayed high cell type specificity could be predicted with >70 % accuracy, while viruses with low cell type specificity could not be predicted above random chance (50 %, marked by the red dashed line). As a negative control, viral presence and absence labels were scrambled at random in the training data, causing the prediction accuracy to drop to random chance (50 %), as expected. The bottom bar plots show the number of testing and training cells for each virus (also see Extended Data Fig. 8c).* ***c****, Heatmap of the prediction accuracy across all possible modeling combinations (training on all macaque genes versus only highly variable (HV) genes, and with or without covariates donor animal and EVD time point). The prediction accuracy remains stable across all modeling choices.*

(ZEBOV), u102540, u11150, and u202260) could be predicted at > 70 % accuracy across models (Fig. 8b and c). The sensitivity and specificity are shown in Extended Data Fig. 8a. By contrast, the presence of viruses that did not display cell type-specificity (u39566, u134800, and u102324) could not be predicted better than random chance (50 %) (Fig. 8b and c). As a negative control, we scrambled the binary virus count matrix used for model training, effectively randomizing the presence or absence of a virus in each cell. As expected, the prediction accuracies dropped to those expected at random (50 %) (Fig. 8b). This learnable relationship between viral presence and host gene expression provides further evidence that reads

from u10, the known infection with ZEBOV, as well as novel viruses u102540, u11150, and u202260, originated from an ongoing viral infection and/or viral clearance which perturbed host gene expression at the single-cell level. Given the cell type specificity of the viruses whose presence could be predicted with high accuracy, we wanted to confirm that we were not simply predicting cell type rather than virus presence. To this end, we performed a second round of modeling whereby virus-negative training cells were selected to be of the same cell types as virus-positive cells. While this slightly decreased prediction accuracy, viruses displaying cell type specificity could still be predicted with greater accuracy than those without (Extended Data Fig. 9c).

We analyzed the top 200 macaque genes with the largest predictive power in the regression model trained on highly variable genes with covariates donor animal and time point. Approximately half of the macaque Ensembl IDs did not have annotated gene names, which is a common problem for genomes from non-model organisms. We used gget[45] to translate annotated Ensembl IDs to gene symbols and to perform enrichment analysis on the returned gene symbols using Enrichr[71] against the GEO microbe perturbations database[72]. The highly weighted genes for all viruses we could predict with high accuracy returned significant enrichment results for microbe perturbations, including many viral infections (Extended Data Fig. 9b). Moreover, we used the human KEGG database to identify predictive genes involved in cellular processes associated with viral infections. Some of the predictive genes were associated with pathways involved in the identification of viral invasion by the innate immune response, such as cytokine-cytokine receptor interactions (CCL24, IL1RL1, IFNG, TGFB3, TNFSF10, INHBB, CCL17 for u10; TNFSF10, PF4 for u102540; ACVRL1, CXCL9, CCL4L1, TNFRSF10A, CCL18 for u11150; IL21, IL10, CXCR1, IL1R2 for u202260), extracellular matrix (ECM) receptor interactions[73] (RELN, VWF, ITGA2, COL6A5 for u10; ITGA2, HMMR for u102540; RELN for u11150; ITGA3, ITGA2B, TNR, ITGA7, CD36, THBS1 for u202260), and the expression of NOD-like receptors[74] (MAPK11, OAS2 for u102540; MAPK11, DHX33, TP53BP1 for u11150; TRPM2, JUN, OAS3 for u202260). Several predictive genes were involved in signaling pathways for the activation and modulation of inflammation, such as IL-17, a key cytokine in neutrophil mobilization[75] (IFNG, CCL17, S100A8 for u10; MAPK11, LCN2, S100A9 for u102540; MAPK11 for u11150; JUN for u202260), Nuclear factor kappa-light-chain-enhancer of activated B cells (NF-κB)[76] (GADD45G for u10; BLNK for u102540; CCL4L1, ERC1, GADD45G for u11150), Peroxisome Proliferator-Activated Receptor gamma (PPAR)[77] (FABP4, CD36 for u202260), and forkhead box O (FoxO)[78] (TGFB3, TNFSF10, IRS2, GADD45G for u10; MAPK11, TNFSF10, IGF1R for u102540; MAPK11, IRS1, IRS2, GADD45G, IGF1R for u11150; IL10 for u202260). Other predictive genes were involved in cellular antiviral responses, such as the induction of inflammatory cell death (apoptosis and necroptosis)[79] (TNFSF10, PRF1, GADD45G, H2AC6, IFNG for u10; CTSL, LMNA, TNFSF10, PRF1, H2AC6 for u102540; CTSL, LMNA, TNFRSF10A, GADD45G, H2AC6 for u11150; JUN, CAMK2B, FTL for u202260), or membrane-associated responses, such as neutrophil extracellular trap formation[80] (SELP, H2AC6, VWF for u10; MAPK11, H2AC6 for u102540; MAPK11, H2AC6, H2BC5 for u11150; ITGA2B for u202260), and Fc gamma R-mediated phagocytosis[81] (PLPP1 for u10; MYO10, PLPP1 for u102540; PLPP1 for u11150).

Discussion

Our work provides a method for extracting a 'virome' modality from any bulk or single-cell RNA-seq data by leveraging a new method that maps and quantifies species-level viral RdRP sequences against an amino acid reference. We built on the existing alignment software kallisto[44] and bustools[84] and expanded them for

translated alignment by (reverse) translating both the amino acid reference and the nucleotide sequencing reads into a common, nonredundant comma-free code. While we validated kallisto translated search in combination with PalmDB for the identification of viral RNA, our novel workflow can be applied in combination with any amino acid reference. kallisto translated search permits the alignment of nucleotide sequencing data to any amino acid reference at single-cell resolution. For example, amino acid sequences of antimicrobial peptides[85] can be used as a reference to identify these peptides in bulk and single-cell RNA sequencing data. Moreover, amino acid transcriptomes of homologous species may be used as a reference for species with missing or incomplete reference genomes. In this case, operating in the amino acid space will increase similarity due to the robustness to single-nucleotide mutations.

We validated kallisto translated search in combination with PalmDB for the detection and identification of viral RNA from up to 10^{12} virus species in next-generation sequencing data at single-cell resolution. As we noted in the introduction, the number of viruses expected to cause human infectious disease is eclipsed by the comparatively few viruses with complete reference genomes and the even smaller number of viruses that have been detected in humans. It is important to monitor the presence of viruses in the human population, both to prevent pandemic outbreaks and to further understand the role of viruses in various diseases. We have shown that such monitoring and novel virus discovery can be performed using single-cell RNA-seq data. Moreover, our work provides a platform for characterizing omnipresent viruses associated with different hosts, thus making possible the compilation of reference viromes from the massive amounts of data in the Sequence Read Archive.

The virus count matrix, which is obtained using kallisto translated search in combination with PalmDB, is an entirely new modality that we have begun to explore in this paper. We found that this matrix is sparse with relatively low molecule counts per cell (Extended Data Fig. 3e). While using the highly conserved RdRP to identify viruses makes our workflow very efficient and is the key to being able to detect up to 10^{12} distinct viruses, RdRP RNA only makes up ~1 % of the total viral RNA present in the sequencing data analyzed here (Extended Data Fig. 2) resulting in the sparsity of the virus count matrix. We anticipate that this number varies between virus species and sequencing technology, making it difficult to define a general detection limit. To normalize this sparse and low-count matrix, we binarized the virus count matrix such that each cell was either positive or negative for each virus. Given the low counts, we expect that there is a high occurrence of false negatives in the virus count matrix while the confidence in positive cells is high. However, we have shown that relationships between viral presence and host gene signatures can be learned regardless.

A common problem in the identification of microbial sequences is the misidentification of host sequences as microbial, as well as differentiating between ongoing infections, reagent or sample contamination, cell-free RNA contamination, endogenous retroviruses, and widespread latent infections. The kallisto translated search method computes both the virus count matrix and the host gene expression matrix at single-cell resolution, providing unique opportunities for parallel analysis of viral signatures and their effect on host gene expression. We describe different approaches to evaluate the nature of viral sequences identified by kallisto translated search, including taxonomic assignment of viruses based on the sOTU, analysis of viral tropism, extraction and BLAST alignment of raw sequencing reads identified as viral, and using a sample spike-in to categorize viruses into shared and sample-specific viruses. Moreover, we describe and evaluate different workflows to mask the host genome and/or transcriptome, allowing different levels of conservativeness and the quantification of sequencing reads that align to viral RdRPs as well as the host

transcriptome. Notably, the efficacy of masking the host genome and/or transcriptome will depend on the quality and comprehensiveness of said genome/transcriptome. In this case, the majority of host sequences originated from rhesus macaque, which has a very comprehensive genome assembly[57]. Finally, we trained logistic regression models to predict viral presence at the single-cell level based on host gene expression, achieving high accuracy indicative of an ongoing viral infection or clearance.

Focusing on the RdRP produces biases between virus species with varying life cycles, depending on the sequencing technology used. The genome of many negative-strand RNA (-ssRNA) is replicated as well as transcribed. Transcription produces short, often polyadenylated mRNA products which are captured and sequenced, including the RdRP. In contrast, the genome of many positive-strand RNA (+ssRNA) viruses undergoes replication, but not transcription. Instead, the genome is translated into polyproteins, which are subsequently cleaved. While +ssRNA virus genomes are often polyadenylated and hence are captured by polyA capture-dependent single-cell RNA sequencing technologies, sequencing ~100 bases from the polyA-tail using a poly(T) primer will not capture the RdRP if it is located too far from the polyA-tail (see the schematic overview of the SARS-CoV genome in Fig. 1). In this scenario, the RdRP of +ssRNA viruses will, however, be captured by bulk RNA sequencing and random hexamer primers in single-cell RNA sequencing (Extended Data Fig. 4c). Hence, sequencing using random hexamer primers overcomes the virus life cycle-dependent bias for single-cell technologies. Many novel sequencing technologies, including Parse Biosciences SPLiT-Seq[33], employ random hexamer primers to produce full-coverage sequencing and overcome biases introduced by poly(T) primers. We foresee that the use of random priming in sequencing will continue to increase. It is worth noting that, depending on the technology, many intra-genomic sequences of +ssRNA viruses will be captured by poly(T) primers nonetheless due to mispriming, as was observed for the +ssRNA virus ZEBOV sequenced with the poly(T) primer-based technology Seq-Well in this paper (Extended Data Fig. 2). Even with random priming, many biases will remain. For example, any viral RNA that is not polyadenylated will not efficiently be captured by single-cell sequencing technologies that rely on polyA capture.

We hope that kallisto translated search will be widely implemented in the analysis of next-generation sequencing data to identify the presence of viral RNA, as well as inform the experimental design of research aiming to identify microbial reads from RNA sequencing data. We describe several experimental design choices that greatly impact the results of microbial read quantification, such as the sequencing primer design and sample spike-ins. The masking workflows described in this paper and the associated challenges are applicable to any metagenomics analysis beyond the identification of viral reads, and the workflows described here can be easily applied to nucleotide references, such as a 16S database for the characterization of the human gut microbiome[86].

Methods

Developing kallisto translated search and optimization for the identification of viral RNA

Building kallisto translated search and choosing a new 'genetic code'

To perform translated alignment, the nucleotide and amino acid sequences need to be translated into a shared 'language'. This might be achieved by translating nucleotides to amino acids or vice versa. Since kallisto encodes nucleotide characters in 2 bits (allowing a total of 4 distinct nucleotides to be encoded), encoding the 20 different amino acids resulting from translated nucleotide sequences was not feasible.

Moreover, reverse translating the amino acid sequences to nucleotides would be intractable due to the redundancy in the genetic code leading to a combinatorial explosion in nucleotide sequences consistent with an amino acid reference. We therefore translated the nucleotide sequences and reverse translated the amino acid sequences using a fixed synthetic code designed to reduce spurious alignments. We explored two different codes for this translation: 1. Comma-free code and 2. A code that maximizes the Hamming distance between frequently occurring amino acids (Extended Data Fig. 10a). While maximizing Hamming distance is advantageous in terms of avoiding sequence multimapping (see next paragraph), a comma-free code prevents off-frame alignment since any k-mers formed by adjacent words will not be included in the dictionary. We found that the comma-free code recalls viral sequences equally well compared to maximizing the Hamming distance between amino acids (Extended Data Fig. 10b).

Optimization of PalmDB for the identification of viral reads in RNA sequencing data

Due to the occurrence of the ambiguous amino acid characters B, J, and Z, 62 out of 296,623 viral sequences were transformed into identical sequences after reverse translation to comma-free code. The identical sequences were merged and assigned a representative virus ID. Due to the high similarity between viral RdRP sequences, the loss of aligned sequences due to multimapping to several reference sequences was a major concern. Moreover, the necessity of reverse translating the amino acid sequences further decreases the Hamming distance between reference sequences by approximately 30 % (Extended Data Fig. 10d). To overcome this problem, we tried clustering the amino acid sequences based on 99 % similarity using the MMseqs2 algorithm[87]. This resulted in 6,518 clusters with high concordance of taxonomy labels between sequences in the same cluster (Extended Data Fig. 10e). However, although clusters were computed correctly based on their concordance with taxonomy, this resulted in 67.4 % of sOTUs not being detected anymore (compared to 3.3 % when using the complete index). As a result, we decided to group the sOTUs instead, treating virus IDs with the same taxonomy across all main taxonomic ranks like transcripts of the same gene (available here: https://tinyurl.com/4wd33rey). This retained the alignment percentage of the complete index while allowing highly accurate taxonomic assignment and minimal sequence loss to multimapping (Fig. 3b). It is noteworthy that the default kallisto k-mer length of 31 nucleotides equals only 10 amino acids. Given the architecture of the current kallisto version (0.50.0), which is optimized for 64-bit k-mers with each nucleotide occupying two bits, k cannot be set > 31. This might change in future versions.

Validation and benchmarks

Visualization of the Kraken2 and kallisto translated search alignments of ZEBOV sequences

Kotliar *et al.*[37] performed single-cell RNA sequencing of PBMC samples from rhesus macaques after infection with ZEBOV (further described below). A subset of the data obtained by Kotliar *et al.* at 8 days post-infection with ZEBOV was used to visualize the identification of RdRP sequences using kallisto (v0.50.0) translated search. The first 100,000,000 raw sequencing reads from the GSE158390 library SRR12698539 were aligned to the ZEBOV reference genome (NC_002549.1) using Kraken2 v2.1.2 and to the optimized PalmDB using kallisto translated search. Aligned reads from both workflows were extracted and realigned to the ZEBOV genome using bowtie2[39] v2.2.5 and SAMtools[40] v1.6 as previously described[88]. The visualization shown in Extended Data Fig. 2 was generated from the resulting sorted bam files with the NCBI Genome Workbench[41].

Testing robustness to mutation

676 *Zaire ebolavirus* (ZEBOV) RdRP sequences were identified by aligning the first 100,000,000 raw sequencing reads from the GSE158390 library SRR12698539 to the optimized PalmDB using kallisto translated search. Mutation-Simulator[48] (v3.0.1) was used to add random single nucleotide base substitutions to the RdRP sequences at increasing mutation rates. We performed 10 rounds of simulated mutations per mutation rate. The sequences were subsequently aligned using kallisto translated search against the complete PalmDB, Kraken2 translated search against the RdRP amino acid sequence of ZEBOV with a manually adjusted NCBI Taxonomy ID to allow compatibility with Kraken2, and kallisto standard workflow against the complete ZEBOV nucleotide genome (GCA_000848505.1). We subsequently calculated the recall percentage over all 676 sequences. For kallisto translated search, the recall percentage was calculated based on species-level taxonomic assignment. Since the other two methods were only given the target virus sequence as a reference and did not have to distinguish between different viruses, their recall percentage was calculated based on all aligned sequences. The recall percentage over all 676 sequences for the 10 rounds at each mutation rate is shown in Fig. 2c. Extended Data Fig. 4b shows the precision with which kallisto translated search identified the correct virus versus other taxonomies at each mutation rate. The recall and precision at mutation rates > 0 were fitted with an inverse sigmoid function using non-linear least squares using the scipy.optimize.curve_fit function (scipy v1.11.1).

Alignment and quantification of viral counts in validation datasets

The sequencing reads for each library used in the validation (Fig. 3a) were aligned with kallisto translated search against the PalmDB index D-listed with the corresponding host genome and transcriptome. The hosts were (i) human (GRCh38 Ensembl version 109) for GSE150316, GSM4548303 and the SARS-CoV-2 saliva, nasal, and throat samples, (ii) mouse (GRCm39 Ensembl version 109) for GSM5974202, and (iii) rhesus macaque (Mmul_10 Ensembl version 109) and dog (ROS_Cfam_1.0 Ensembl version 109) for GSE158390. Count matrices were generated with bustools (v0.43.1). Fig. 3a shows the total raw counts obtained for each target virus species. RT-qPCR and RNA-ISH counts were reproduced from the original publications.

Validating the alignment of nucleotide sequences to an amino acid reference and assessing the accuracy of the taxonomic assignment

To validate the mapping of nucleotide sequences to an amino acid reference with kallisto translated search and assess the accuracy of the taxonomic assignment, we reverse translated all amino acid sequences in the PalmDB using the 'standard' genetic code from the biopython[89] (v1.79) Bio.Data.CodonTable module and DnaChisel[90] (v3.2.10) (with a slight adaptation to allow the ambiguous amino acids 'X', 'B', 'J', and 'Z' occurring in the PalmDB, which was later implemented in DnaChisel v3.2.11). A unique synthetic 'cell barcode' was generated for each resulting nucleotide sequence, and the sequences were aligned to the optimized amino acid PalmDB with kallisto translated search, keeping track of each sequence separately as if they were an individual cell. The synthetic barcodes allowed subsequent analysis of the alignment result for each individual sequence, and the accuracy of the obtained taxonomy based on the virus ID to sOTU mapping provided by PalmDB is shown in Fig. 3b. For each sequence, we differentiated between 'correct' or 'incorrect' taxonomic assignment, or, if the sequence did not return any results, whether it was 'multimapped' (the sequence aligned to multiple targets in the reference and could not unambiguously be assigned to one) or 'not aligned' (the sequence was not aligned), at each taxonomic rank.

Analysis of macaque PBMC data

Kotliar *et al.*[37] performed single-cell RNA sequencing of PBMC samples from 19 rhesus macaques at different time points during Ebola virus disease (EVD) after infection with ZEBOV (EBOV/Kikwit; GenBank accession MG572235.1; *Filoviridae: Zaire ebolavirus*) using Seq-Well[82] with the S3 protocol[83]. A subset of PBMC samples were spiked with Madin-Darby canine kidney (MDCK) cells. The data is available at GSE158390, and we obtained the raw sequencing data from the European Nucleotide Archive using FTP download links. The data is split into 106 datasets containing 30,594,130,037 reads in total.

Alignment to the host transcriptome

The rhesus macaque Mmul_10 and domestic dog ROS_Cfam_1.0 genomes were retrieved from Ensembl version 109. The reference index was built using both genomes and the kb-python (v0.28.0 with kallisto v0.50.0 and bustools v0.43.1) ref command to create a combined index containing the transcriptome of both species. We quantified the gene expression in each of the 106 datasets using the standard kallisto-bustools workflow[13] with the 'batch' and 'batch-barcodes' arguments to process all files simultaneously while keeping track of each batch, and with the 'x'-string '0,0,12:0,12,20:1,0,0' to match the Seq-Well technology. Since the Seq-Well technology does not provide a barcode on-list, we generated a barcode on-list using the 'bustools allowlist' command, requiring each barcode to occur at least 1,000 times. We subsequently corrected the cell barcodes using the generated on-list and computed the count matrix using the 'bustools count' function.

Host cell quality control, filtering, and separation of macaque and MDCK cells

The count matrix generated by bustools was converted to h5ad using kb_python.utils.kb_utils and read into Python using anndata v0.8.0. Metadata such as donor animal, the presence of an MDCK spike-in, and time point were added to the AnnData object from the SRR library metadata provided by Kotliar *et al.*[37]. The cell barcodes were filtered based on a minimum number of UMI counts of 125 obtained from the knee plot of sorted total UMI counts per cell (Extended Data Fig. 3a), resulting in a mean UMI count of 1,401 after filtering. The cells were further filtered based on a maximum percentage of mitochondrial genes of 10 %, based on a combination of macaque and dog mitochondrial genes facilitated by Scanpy[91] (v1.9.3) and gget[45] (v0.28.0). Cells were categorized as macaque if a maximum of 10 % of their UMIs originated from dog genes and vice versa (Extended Data Fig. 3b). Macaque and MDCK cells were normalized separately using log(CP10k + 1) with Scanpy's normalize_total defaults of target sum 10,000 and log1p.

Macaque cell clustering and cell type assignment

The macaque gene count matrix was transformed by PCA to 50 dimensions applied using the log-normalized counts filtered for highly variable genes using Scanpy's highly_variable_genes. Next, we computed nearest neighbors and conducted Leiden clustering[58] using Scanpy, resulting in 19 Leiden clusters. We found that EVD time points were highly concordant across sequencing libraries, suggesting the lack of a batch effect (Fig. 7a, also see GitHub code repository). Each cluster was manually annotated with a cell type based on the expression of previously established marker genes[37] (Extended Data Fig. 3d). Cluster 'Undefined 1' was omitted because it only contained 12 cells. Gene names and descriptions for Ensembl IDs without annotations were obtained using gget[45].

Virus alignment with different masking options

For each masking option, we quantified the gene expression in each of the 106 datasets from GSE158390 using kallisto with the 'batch' and 'batch-barcodes' arguments to process all files simultaneously while keeping track of each batch and with the 'x'-string '0,0,12:0,12,20:1,0,0' to match the Seq-Well technology. kallisto translated search was initiated in the 'kallisto index' and 'kallisto bus' commands by adding the '—aa' flag. Following the alignment to PalmDB with any of the masking options, cell barcodes were corrected using the barcode on-list generated during the alignment to the host as described above.

- No mask

The raw sequencing reads were aligned to the optimized PalmDB reference files (see 'Optimization of PalmDB' above) using kallisto translated search.

- D-list genome + transcriptome

The raw sequencing reads were aligned to the optimized PalmDB reference using kallisto translated search with the added argument 'd-list', which was passed the concatenated macaque genome and transcriptome (Mmul_10 Ensembl version 109), and dog genome and transcriptome (ROS_Cfam_1.0 Ensembl version 109). For D-list masking options including only the genomes or transcriptomes (Extended Data Fig. 4a), only the genome or transcriptome files from both species were concatenated and passed to the 'd-list' argument, respectively.

- D-list genome + transcriptome + ambiguous reads filtered

This workflow was performed as described above for the 'D-list genome + transcriptome' with an unreleased version of kallisto where ambiguous reads in the D-list will be thrown out as host instead of being assigned to virus (Extended Data Fig. 4a). We explored this option to investigate the effect of ambiguous reads during D-list masking. However, we found that the alignment results did not notably differ from the masking option 'D-list genome + transcriptome' (Fig. 4a and Extended Data Fig. 5).

- Host read capture with kallisto

The raw sequencing reads were aligned to the combined macaque and dog reference index generated during the alignment to host with 'kallisto bus' with the added '-n' flag. The '-n' flag keeps track of the read line number of each aligned read; the line numbers are added to the resulting bus file. The raw sequencing reads were also aligned to the modified PalmDB with kallisto translated search with the added '-n' flag to obtain all reads that map to viral RdRPs. Subsequently, the bus file returned by kallisto translated search was split into reads that only aligned to viral RdRPs and reads that also aligned to host based on the read line numbers in the bus files. This step was performed using 'bustools capture' to, first, obtain all reads that belonged to a single batch file (of the 106 dataset files), and, second, capture all reads that also aligned to host.

- Host read capture with kallisto + D-list genome + transcriptome

Host reads were captured with kallisto as described above under 'Host read capture with kallisto'. However, during the alignment of the raw sequencing reads to PalmDB with the '-n' flag, we also used the 'd-list' flag to mask the host genomes and transcriptomes as described above under 'D-list genome + transcriptome'.

- Prior alignment to host with bwa

bwa[54] v0.7.17 was installed from source. The 'bwa index' command was used to generate a bwa index from the concatenated macaque and dog genomes (Mmul_10 and ROS_Cfam_1.0 from Ensembl v109). The raw

sequencing reads were subsequently aligned to the bwa index using the 'bwa mem' command, aligning each file separately. For each FASTQ file, the names of all unmapped reads were extracted using 'samtools view' (SAMtools[40] v1.6), and a new FASTQ file including only unmapped sequences was generated using the 'seqtk subseq' command (v1.4; https://github.com/lh3/seqtk). The resulting FASTQ files containing the sequencing reads that did not map to the host genomes were aligned to the optimized PalmDB reference files using kallisto translated search.

Extraction and BLAST alignment of viral reads

Randomly selected sequencing reads from three libraries that included reads that mapped to the viruses of interest were aligned to the optimized PalmDB with kallisto translated search including the '-n' flag, without any host read masking. Reads that mapped to the viruses of interest were subsequently captured and extracted from the raw sequencing FASTQ files using 'bustools capture' and 'bustools extract'.

BLAST+[55,56] v2.14.1 was installed from source and the BLAST nt database was downloaded using the update_blastdb.pl command. 10 reads were randomly chosen for each target virus for each library and were BLASTed against the nt database using the blastn algorithm. Sequences that aligned to the polyA tail were recognized by the occurrence of 'AAAAAAAAAAAA' or 'TTTTTTTTTTTT' in the aligned part of the subject or query sequences and removed from the results. BLAST results were subsequently plotted using pyCirclize.Circos (v1.0.0; https://github.com/moshi4/pyCirclize).

Virus quality control

The viral count matrix generated using the 'Host read capture with kallisto + D-list genome + transcriptome' masking workflow was converted to h5ad using kb_python.utils.kb_utils and read into Python using anndata v0.8.0. Metadata such as donor animal, the presence of an MDCK spike-in, and time point were added to the AnnData object from the SRR library metadata provided by Kotliar *et al.*[37]. For each cell, the host species and cell type were added from the host matrices generated as described above. The virus count matrix was subsequently binarized, such that for each cell, each virus was either present or absent. The viruses were thresholded to viruses that were observed in ≥ 0.05 % of cells in either species.

Virus categorization into shared, 'macaque only', and 'MDCK only' viruses

For each virus ID, the virus was defined as 'shared' if the fold change between the fraction of positive macaque cells and the fraction of positive MDCK cells was less than or equal to 2. Viruses were assigned the category 'macaque only' if the virus was seen in ≥ 0.05 % of macaque cells and ≤ 7 MDCK cells, and vice versa for the category 'MDCK only'. These thresholds were defined based on the percentages of positive cells observed for each virus in each species, as shown in Fig. 6b.

Generation of the Krona plot

KronaTools[62] v2.8.1 was installed from source. We generated a data frame containing the total numbers of positive cells for each sOTU seen in ≥ 0.05 % of macaque cells for each animal and time point (including only cells that passed host cell quality control). The ktImportText tool was used to generate a Krona plot HTML file from a text file generated from this data frame.

Logistic regression models to predict viral presence based on host gene expression

Logistic regression models the log odds ratio of an event as a weighted linear combination of some predictor variables. That is, the natural log of the ratio of the probability p that an event occurs to the probability that it does not occur is modeled:

$$ln\left(\frac{p}{1-p}\right) = \sum_{i=1}^{N} \beta_i x_i + \beta_0,$$

where each x_i is a predictor variable with corresponding weight β_i and β_0 is an intercept. Here, p is the probability of viral presence or absence in a given cell, predicted based on a linear combination of normalized host gene count values (denoted as x with a total of G modeled genes). Viral presence or absence is modeled for a single virus at a time. To control for covariates, we also included animal identifier (denoted as y with a total of A animals) and time point (denoted as z with a total of T time points), which were one-hot encoded for fits:

$$ln\left(\frac{p}{1-p}\right) = \beta_0 + \sum_{g\in G} \beta_g^G x_g + \sum_{a\in A} \beta_a^A y_a + \sum_{t\in T} \beta_t^T z_t$$

The magnitude of the weight value for each predictor variable corresponds to that variable's influence on event probability, with large positive weights increasing the probability and large negative weights decreasing the probability of the event. Thus, for our purposes, an analysis of gene weights suggests which genes are likely to correlate with viral infection. For models parameterized by highly variable (HV) genes, the host (macaque) matrix was subset to highly variable genes as defined above. To reduce the occurrence of false negative viral counts, the logistic regression models were trained using the viral count matrix obtained without any masking of the host genes. However, the models were trained for viruses that were filtered based on the more conservative masking options ('macaque only' and 'shared' viruses).

For viruses with more virus-negative than virus-positive cells, half of the virus-positive cells and an equal number of virus-negative cells were randomly selected to train the logistic regression models. For viruses with more virus-positive than virus-negative cells, half of the virus-negative cells and an equal number of virus-positive cells were randomly selected for training. In both cases, the remaining cells were held out for testing the performance of trained models. The number of training and testing cells for each virus are shown in Extended Data Fig. 8c. For models that included covariates, donor animal and EVD time point were one-hot encoded and appended to the gene expression training matrix. All models included an intercept. Models were trained with L2 weight regularization using the sklearn.linear_model.LogisticRegression (sklearn v1.0.1) classifier with a maximum of 100 iterations to predict the probability of viral presence at single-cell resolution. Virus-positive cells were assigned class label 1, and virus-negative cells were assigned class label 0. All four possible combinations of two modeling choices (highly variable versus all genes, and covariates versus no covariates) were tested, and the results are shown in Fig. 8c. Accuracy, specificity, and sensitivity were calculated for each model on the held-out testing cells (Extended Data Fig. 8a). A negative control where labels of viral presence and absence for each virus were randomly scrambled in the training data was included in the modeling experiments. For the scrambled labels, the original ratio of virus-positive to virus-negative cells was maintained.

Given the cell type specificity of the viruses whose presence could be predicted with high accuracy, we wanted to confirm that we were not simply predicting cell type. To this end, we performed a second round of modeling whereby virus-negative training cells were selected to be of the same cell types as virus-positive cells (Extended Data Fig. 9c and d). To further reduce the occurrence of false negative viral counts in these models, we filtered the virus and host matrices to include only the top 50 % of cells according to the sum of raw host reads per cell before training the models. This was done to reduce the effects introduced

by varying sequencing depths. For example, cells with a lower sequencing depth will have a higher likelihood of a false negative viral count.

Enrichment analysis of predictive genes

We analyzed the top 200 macaque genes with the largest positive weights in the regression model trained on highly variable genes with covariates donor animal and time point. The gene weight distributions are shown in Extended Data Fig. 9a. Approximately half of the macaque Ensembl IDs did not have annotated gene names. We used gget[45] to translate annotated Ensembl IDs to gene symbols and to perform enrichment analysis on the returned gene symbols using Enrichr[71] against the GEO microbe perturbations database ('Microbe_Perturbations_from_GEO_up')[72]. The reported P values were corrected with the Benjamini-Hochberg method.

Data availability

Sample	Methods	Data shown in	DOI	GEO accession
Lung autopsy samples from COVID-19 patients	Bulk RNA sequencing; RNA-ISH	Fig. 3a	https://doi.org/10.1038/s41467-020-20139-7	GSE150316
Self-collected saliva, anterior nares swab, and oropharyngeal swab samples from individuals enrolled in a COVID-19 household transmission study	Bulk RNA sequencing with viral surveillance panel enrichment (Illumina Cat. 20040536 and 20088154); RT-qPCR	Fig. 3a	https://doi.org/10.1128/spectrum.03873-22 https://doi.org/10.1093/pnasnexus/pgad033	Raw sequencing data is not publicly available per participant privacy practices
SARS-CoV-2 infected human iPSC derived cardiomyocytes	SMART-Seq V4	Fig. 3a	https://doi.org/10.1016/j.xcrm.2020.100052	GSM4548303
Blood samples from rhesus macaques infected with *Zaire ebolavirus*	Seq-Well S^3; RT-qPCR	Fig. 2-8; Extended Data Fig. 1-9	https://doi.org/10.1016/j.cell.2020.10.002	GSE158390
Lungs from APOE knock-in mice infected with SARS-CoV-2	SPLiT-Seq (Parse Biosciences)	Extended Data Fig. 4c	https://doi.org/10.1038/s41586-022-05344-2	GSM5974202

Table 1: *Availability of data analyzed in this paper.*

File	Description	Category
host alignment results.zip	Raw alignment results obtained by kallisto after alignment to the macaque and dog (to account for the MDCK spike-in) transcriptomes	Alignment of the macaque PBMC data[37] to the host transcriptome(s)
host QC.h5ad	Filtered count matrix containing all host cells	
canis QC norm leiden.h5ad	Filtered and clustered count matrix containing MDCK cells	
macaque QC norm leiden.h5ad	Filtered and clustered count matrix containing macaque cells	
macaque QC norm leiden celltypes.h5ad	Filtered and clustered count matrix containing macaque cells with cell type assignments	
virus no mask alignment results.zip	Raw alignment results obtained by kallisto translated search after alignment to the PalmDB without masking host sequences	Alignment of the macaque PBMC data[37] to the PalmDB for the detection of viral RNA with different workflows for the masking of host genome(s) and transcriptome(s)
virus no mask.h5ad	Count matrix obtained through the alignment above with added metadata	
virus dlist cdna alignment results.zip	Raw alignment results obtained by kallisto translated search after alignment to the PalmDB while masking host transcriptome(s) using the D-list	
virus dlist cdna.h5ad	Count matrix obtained through the alignment above with added metadata	
virus dlist dna alignment results.zip	Raw alignment results obtained by kallisto translated search after alignment to the PalmDB while masking host genome(s) using the D-list	
virus dlist dna.h5ad	Count matrix obtained through the alignment above with added metadata	
virus dlist cdna dna alignment results.zip	Raw alignment results obtained by kallisto translated search after alignment to the PalmDB while masking host genome(s) and transcriptome(s) using the D-list	
virus dlist cdna dna.h5ad	Count matrix obtained through the alignment above with added metadata	
virus dlist cdna dna amb alignment results.zip	Raw alignment results obtained by kallisto translated search after alignment to the PalmDB while masking host genome(s) and transcriptome(s) using the D-list + forcing ambiguous sequences to be discarded	
virus dlist cdna dna ambiguous.h5ad	Count matrix obtained through the alignment above with added metadata	
virus host capture alignment results.tar.gz	Raw alignment results obtained by kallisto translated search after alignment to the PalmDB + reads that align to the host transcriptome(s) were captured	
virus host-captured.h5ad	Count matrix obtained through the alignment above with added metadata	
virus host capture dlist cdna dna alignment results.tar.gz	Raw alignment results obtained by kallisto translated search after alignment to the PalmDB while masking host genome(s) and transcriptome(s) using the D-list + reads that align to the host transcriptome(s) were captured	
virus host-captured dlist cdna dna.h5ad	Count matrix obtained through the alignment above with added metadata	
bwa unmapped reads.tar.gz	Raw sequencing files obtained after removal of host sequences based on alignment with bwa	
virus bwa alignment results.zip	Raw alignment results obtained by kallisto translated search after alignment to the PalmDB after reads that align to the host genome(s) with bwa were removed	
virus bwa.h5ad	Count matrix obtained through the alignment above with added metadata	
supp viruses all genes fullM cov none l2.pickle	Model built for all 'macaque only' and 'shared' viruses using all macaque genes and all cells without covariates.	Logistic regression models to predict viral presence based on host gene expression
supp viruses all genes fullM cov donor time l2.pickle	Model built for all 'macaque only' and 'shared' viruses using all macaque genes and all cells with covariates donor animal and EVD time point.	
supp viruses hv genes fullM cov none l2.pickle	Model built for all 'macaque only' and 'shared' viruses using highly variable macaque genes and all cells without covariates.	
supp viruses hv genes fullM cov none l2 scramble.pickle	Model built for all 'macaque only' and 'shared' viruses using highly variable macaque genes and all cells without covariates. Viral presence and absence labels were scrambled in the training data.	
supp viruses hv genes fullM cov donor time l2.pickle	Model built for all 'macaque only' and 'shared' viruses using highly variable macaque genes and all cells with covariates donor animal and EVD time point.	
supp viruses hv genes fullM cov donor time l2 scramble.pickle	Model built for all 'macaque only' and 'shared' viruses using highly variable macaque genes and all cells with covariates donor animal and EVD time point. Viral presence and absence labels were scrambled in the training data.	
top7 viruses all genes fullM cov donor time l2 equalprop.pickle	Model built for the 7 viruses shown in the main figures using all macaque genes and all cells with covariates donor animal and EVD time point.	
top7 viruses hv genes fullM cov donor time l2 equalprop.pickle	Model built for the 7 viruses shown in the main figures using highly variable macaque genes and all cells with covariates donor animal and EVD time point.	
top7 viruses hv genes fullM cov donor time l2 equalprop scramble.pickle	Model built for the 7 viruses shown in the main figures using highly variable macaque genes and all cells with covariates donor animal and EVD time point. Viral presence and absence labels were scrambled in the training data.	
top7 viruses all genes halfM cov donor time l2 equalprop.pickle	Model built for the 7 viruses shown in the main figures using all macaque genes and 50 % of cells with the highest sequencing depth with covariates donor animal and EVD time point.	
top7 viruses hv genes halfM cov donor time l2 equalprop.pickle	Model built for the 7 viruses shown in the main figures using highly variable macaque genes and 50 % of cells with the highest sequencing depth with covariates donor animal and EVD time point.	
top7 viruses hv genes halfM cov donor time l2 equalprop scramble.pickle	Model built for the 7 viruses shown in the main figures using highly variable macaque genes and 50 % of cells with the highest sequencing depth with covariates donor animal and EVD time point. Viral presence and absence labels were scrambled in the training data.	
palmdb human dlist cdna dna.idx	Pre-computed PalmDB reference index with human genomic and transcriptomic sequences masked using D-list	Pre-computed references for future use with kallisto translated search
palmdb mouse dlist cdna dna.idx	Pre-computed PalmDB reference index with mouse genomic and transcriptomic sequences masked using D-list	

Table 2: *Availability of data generated in this paper. The data is available on Caltech Data under the DOI 10.22002/sh33z-hrx98.*

The PalmDB reference files optimized for use with kallisto translated search for the identification of viral sequences in bulk and single-cell RNA sequencing data are available here: https://tinyurl.com/4wd33rey.

Code availability

The code used to generate all of the results and figures reported in this paper, starting from the raw data, can be found here: https://github.com/pachterlab/LSCHWCP_2023. The code is organized by figure panel and provided in immediately executable Google Colab notebooks to maximize the reproducibility of the results and methods described in this manuscript.

Acknowledgments

We would like to thank Astrid Bryon for her advice and helpful discussions on the applicability of kallisto translated search for the detection of viral RNA. We would like to thank Aaron Lin, Lisa Hensley, Dylan Kotliar, and Pardis Sabeti for helping us understand and work with their data. The illustrations in Figures 1, 4, and 6 were created with BioRender.com.

Funding

LL was supported by funding from the Biology and Bioengineering Division at the California Institute of Technology. DKS was supported by funding from the UCLA-Caltech Medical Scientist Training Program (NIH NIGMS training grant T32 GM008042). AVW was supported by NIH F30AI167524.

Ethics declarations

Competing Interests: The authors declare no competing interests.

Extended Data

Virus ID	Phylum	Class	Order	Family	Genus	Species
u102540	Pisuviricota	Pisoniviricetes	Nidovirales	*Coronaviridae*	*Alphacoronavirus*	.
u10	Negarnaviricota	Monjiviricetes	Mononegavirales	*Filoviridae*	*Ebolavirus*	*Zaire ebolavirus*
u10240	Pisuviricota	Pisoniviricetes	Nidovirales	*Arteriviridae*	.	.
u1001	Negarnaviricota	Insthoviricetes	Articulavirales	*Orthomyxoviridae*	*Alphainfluenzavirus*	*Influenza A virus*
u100291	Negarnaviricota	Monjiviricetes	Mononegavirales	.	.	.
u103829	Negarnaviricota	Insthoviricetes	Articulavirales	*Orthomyxoviridae*	.	.
u110641	Duplornaviricota	Resentoviricetes	Reovirales	*Reoviridae*	.	.
u101227	Pisuviricota	Pisoniviricetes	Picornavirales	*Picornaviridae*	.	.
u100188	Kitrinoviricota	Alsuviricetes	Martellivirales	*Closteroviridae*	.	.
u27694	Peploviricota	Herviviricetes	Herpesvirales	*Herpesviridae*	*Varicellovirus*	*Bubaline alphaherpesvirus 1*
u100245	.	.	.	*Fusariviridae*	.	.
u10015	Duplornaviricota	Chrymotiviricetes	Ghabrivirales	*Totiviridae*	.	.
u100733	Negarnaviricota	.	.	.	.	.
u100173	Lenarviricota	Miaviricetes	Ourlivirales	*Botourmiaviridae*	*Ourmiavirus*	.
u100196	Negarnaviricota	Monjiviricetes	.	.	.	.
u100599	Negarnaviricota	Ellioviricetes	.	.	.	.
u100644	Lenarviricota	Amabiliviricetes	Wolframvirales	.	.	.
u100296	Pisuviricota	Pisoniviricetes	Picornavirales	*Dicistroviridae*	.	.
u100017	Lenarviricota	Allassoviricetes	Levivirales	*Leviviridae*	.	.
u100002	Lenarviricota	Allassoviricetes	Levivirales	.	.	.
u100012	Lenarviricota	Allassoviricetes	.	.	.	.
u100024	Pisuviricota	Duplopiviricetes	Durnavirales	*Picobirnaviridae*	.	.
u100048	Lenarviricota	Amabiliviricetes	.	.	.	.
u100302	Negarnaviricota	Monjiviricetes	Mononegavirales	*Rhabdoviridae*	.	.
u100074	Lenarviricota	Howeltoviricetes	Cryppavirales	.	.	.
u100289	Negarnaviricota	Ellioviricetes	Bunyavirales	.	.	.
u100026	Pisuviricota	Duplopiviricetes	Durnavirales	.	.	.
u100111	Duplornaviricota	Chrymotiviricetes	Ghabrivirales	.	.	.
u100139	Kitrinoviricota	Alsuviricetes	Martellivirales	.	.	.
u100154	Pisuviricota	Duplopiviricetes	Durnavirales	*Amalgaviridae*	.	.
u100251	Pisuviricota	Duplopiviricetes	.	.	.	.
u100177	Kitrinoviricota	Tolucaviricetes	Tolivirales	.	.	.
u100215	Duplornaviricota	Chrymotiviricetes	.	.	.	.
u100049	Lenarviricota	Miaviricetes	.	.	.	.
u100000	Kitrinoviricota	Tolucaviricetes	Tolivirales	*Tombusviridae*	.	.
u100001	Lenarviricota	Howeltoviricetes	Cryppavirales	*Mitoviridae*	.	.
u100007	Lenarviricota	.	.	.	.	.
u100004	Lenarviricota	Miaviricetes	Ourlivirales	.	.	.
u100011	Lenarviricota	Howeltoviricetes	.	.	.	.
u100093	Pisuviricota	Duplopiviricetes	Durnavirales	*Partitiviridae*	.	.
u100116	Pisuviricota	Pisoniviricetes	.	.	.	.
u100019	Pisuviricota	Duplopiviricetes	Durnavirales	*Picobirnaviridae*	*Picobirnavirus*	.
u100076	Kitrinoviricota	Tolucaviricetes	.	.	.	.
u100028	Pisuviricota	.	.	.	.	.
u100153	Lenarviricota	Miaviricetes	Ourlivirales	*Botourmiaviridae*	.	.
u100031	Kitrinoviricota	Alsuviricetes	.	.	.	.
u100145	Pisuviricota	Pisoniviricetes	Sobelivirales	.	.	.
u102324	Pisuviricota	Pisoniviricetes	Picornavirales	*Iflaviridae*	.	.

Extended Data Table 1: *Virus ID to species-like operational taxonomic unit (sOTU) mapping for the most highly expressed viruses (in the same order as shown in Fig. 6d). Virus IDs that are further mentioned in the paper are marked in blue. Virus IDs not included in this list are of unknown taxonomy across all taxonomic ranks.*

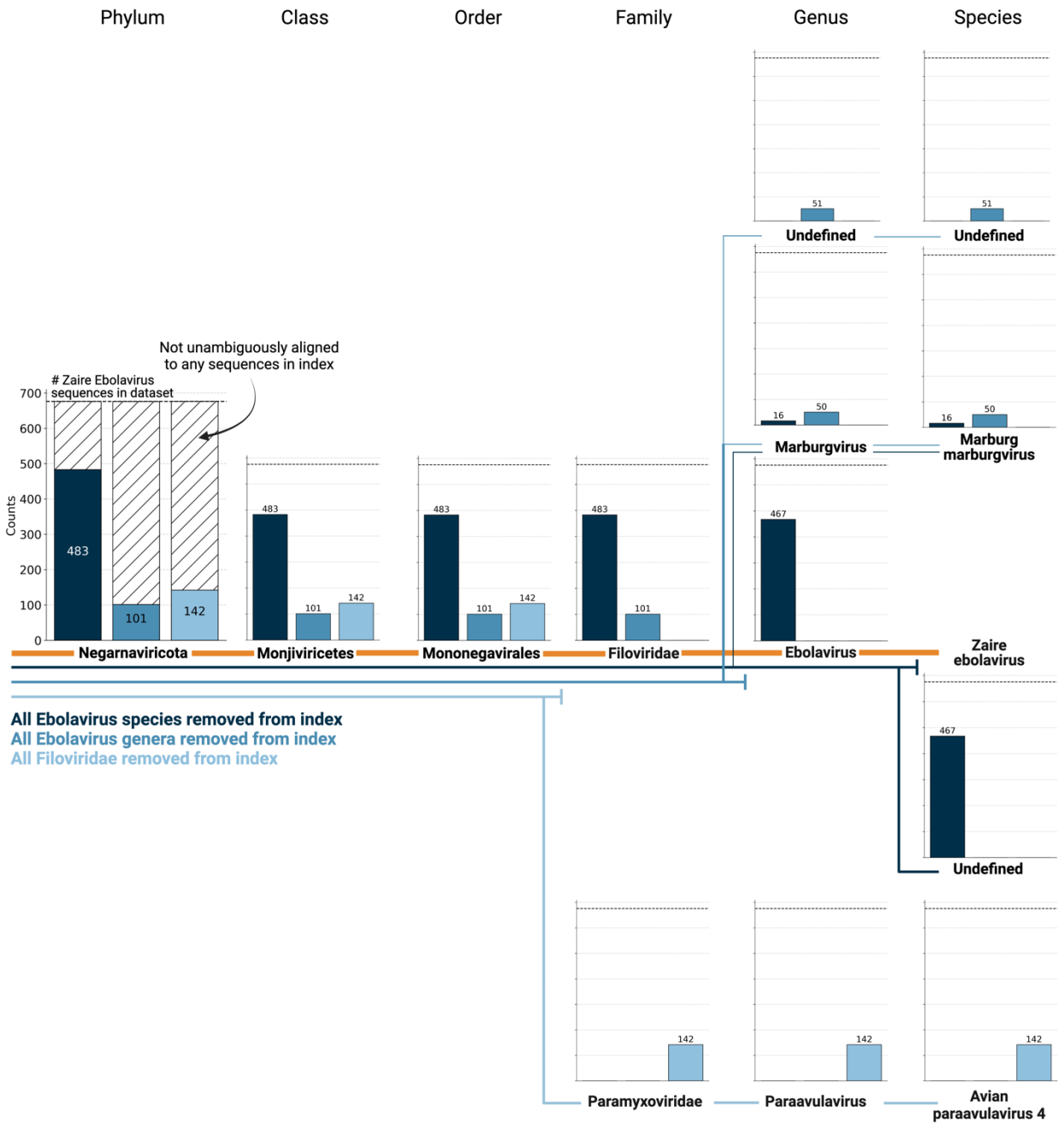

Extended Data Fig. 1: *676 ZEBOV RdRP sequences were identified by aligning a subset of 100,000,000 single-cell RNA sequencing reads of macaque PBMC samples obtained at 8 days post-infection with ZEBOV*[37] *to the optimized PalmDB using kallisto translated search. We subsequently aligned the sequences to PalmDB reference indices from which (i) all Ebolavirus species were removed (dark blue), (ii) all Ebolavirus genera were removed (medium blue), or (iii) all Filoviridae were removed (light blue). In each scenario, a subset of sequences aligned to the nearest remaining relative based on the main taxonomic rank, suggesting that kallisto translated search can detect the highly conserved RdRP of a large number of viral species, beyond the number of sequences in the PalmDB database, while still providing reliable sOTU-based taxonomic assignment of lower-rank taxonomies.*

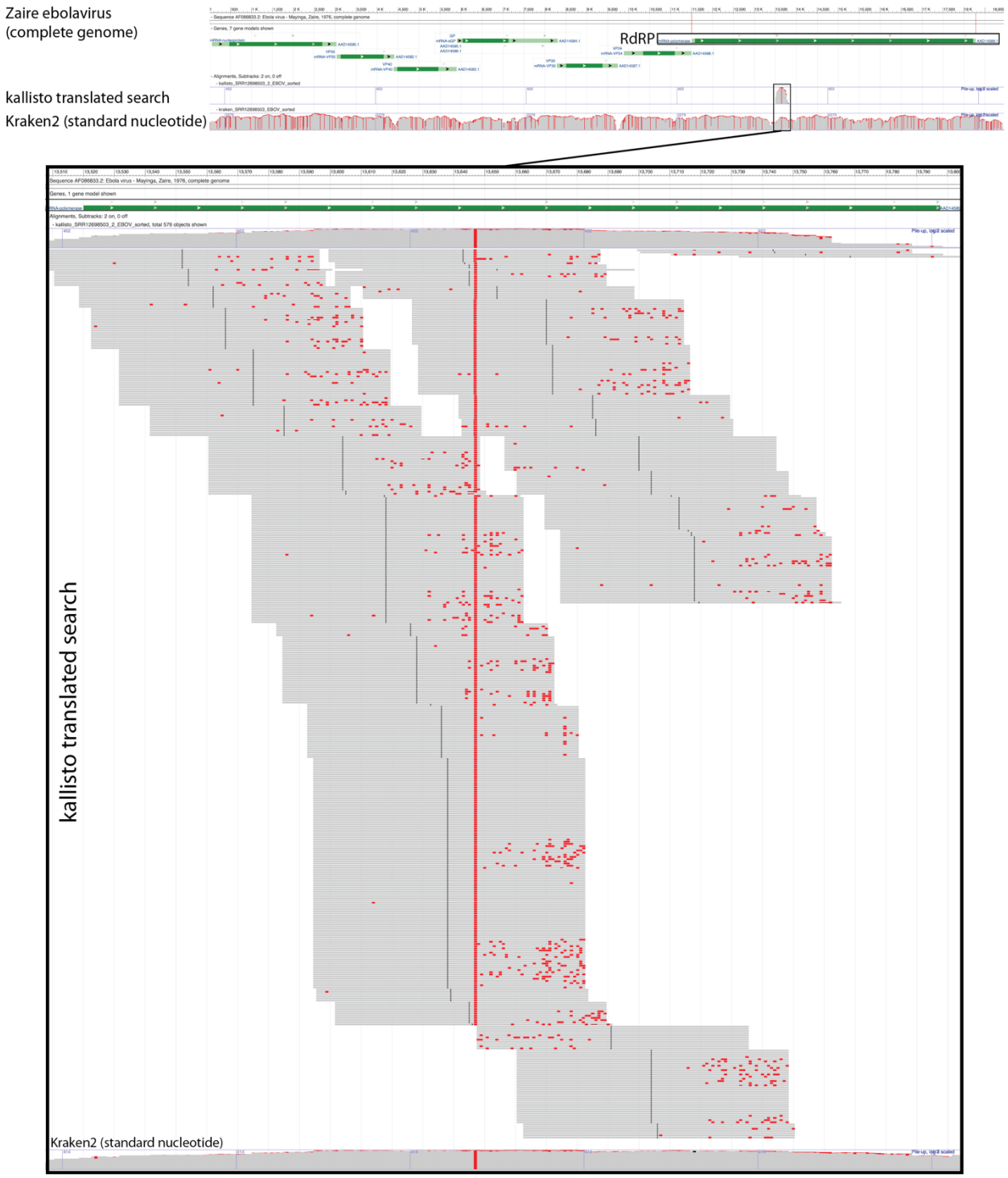

Extended Data Fig. 2: *Visualization of the identification of RdRP sequences with kallisto translated search. We selected a subset of 100,000,000 reads obtained using Seq-Well sequencing of macaque peripheral blood mononuclear cell (PBMC) samples obtained at 8 days post-infection with ZEBOV[37]. We aligned the reads to the PalmDB amino acid sequences with kallisto translated search. We also aligned the reads to the complete ZEBOV nucleotide genome using Kraken2 (standard nucleotide alignment)[27]. Aligned reads from both alignments were extracted and realigned to the ZEBOV genome using bowtie2[39], a BAM file was created using SAMtools[40], and the alignment was subsequently visualized NCBI Genome Workbench[41].*

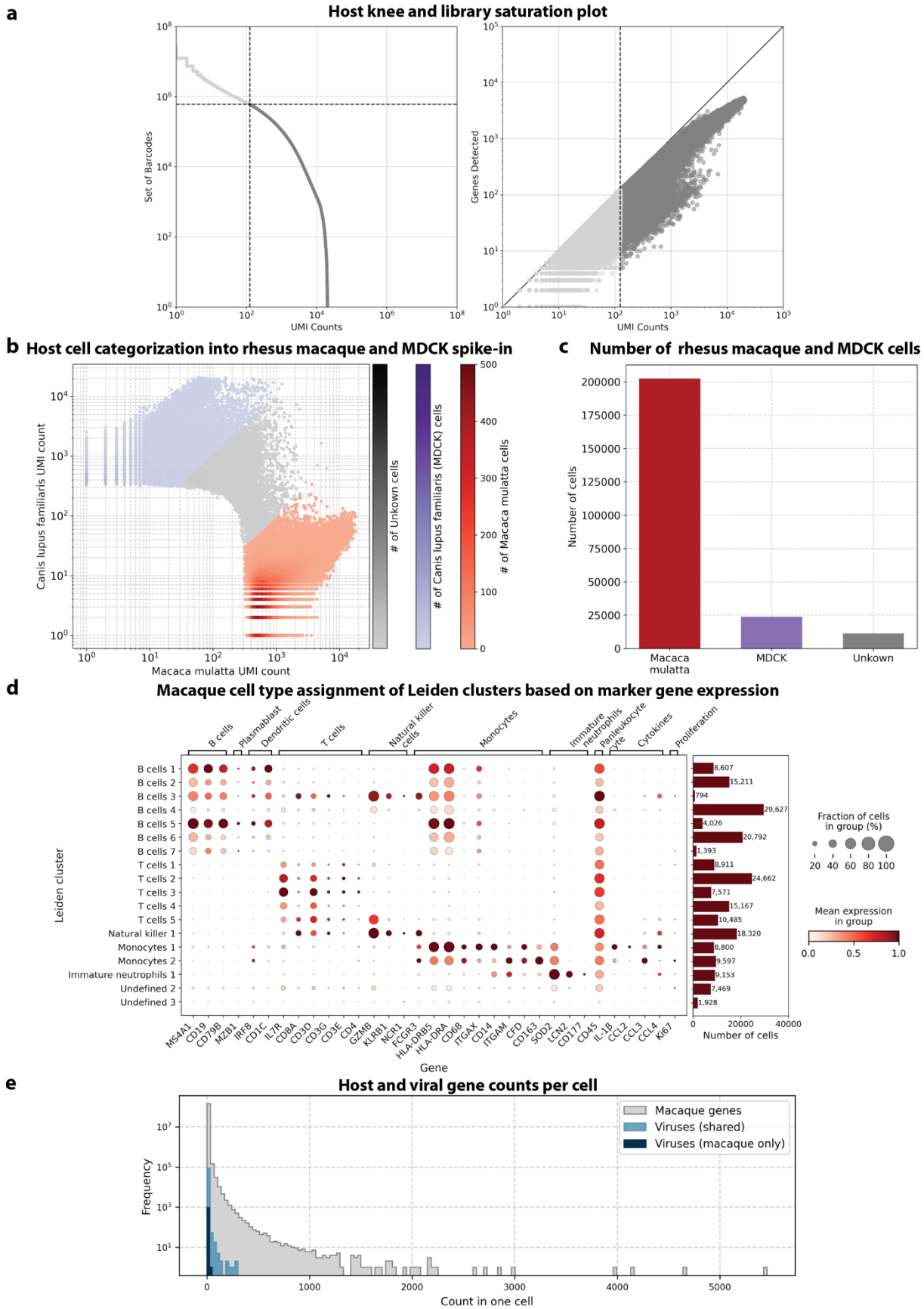
a
Host knee and library saturation plot
Set of Barcodes
UMI Counts
Genes Detected
UMI Counts
b
Host cell categorization into rhesus macaque and MDCK spike-in
Canis lupus familiaris UMI count
Macaca mulatta UMI count
# of Unkown cells
# of Canis lupus familiaris (MDCK) cells
# of Macaca mulatta cells
c
Number of rhesus macaque and MDCK cells
Number of cells
Macaca mulatta
MDCK
Unkown
d
Macaque cell type assignment of Leiden clusters based on marker gene expression
B cells
Plasmablast
Dendritic cells
T cells
Natural killer cells
Monocytes
Immature neutrophils
Panleukocyte
Cytokines
Proliferation
Leiden cluster
B cells 1
B cells 2
B cells 3
B cells 4
B cells 5
B cells 6
B cells 7
T cells 1
T cells 2
T cells 3
T cells 4
T cells 5
Natural killer 1
Monocytes 1
Monocytes 2
Immature neutrophils 1
Undefined 2
Undefined 3
MS4A1
CD19
CD79B
MZB1
IRF8
CD1C
IL1R
CD8A
CD3D
CD3G
CD3E
CD4
GZMB
KLRB1
NCR1
FCGR3
HLA-DRB5
HLA-DRA
CD68
ITGAX
CD14
ITGAM
CFD
CD163
SOD2
LCN2
CD177
CD45
IL-1B
CCL2
CCL3
CCL4
Ki67
Gene
Number of cells
Fraction of cells in group (%)
Mean expression in group
e
Host and viral gene counts per cell
Macaque genes
Viruses (shared)
Viruses (macaque only)
Frequency
Count in one cell

Extended Data Fig. 3: a*, Knee plot of sorted total UMI counts per cell and library saturation plot of host (rhesus macaque and MDCK) cells sequenced by Kotliar et al.*[37] ***b,*** *Canis lupus (dog/MDCK) over Macaca mulatta (macaque) UMI count for each cell. Cells were categorized as macaque if a maximum of 10 % of their UMIs originated from dog genes and vice versa.* ***c****, The obtained numbers of macaque, dog (MDCK), and uncategorized cells after species separation.* ***d****, Mean expression of marker genes used for cell type assignment per macaque Leiden cluster. The barplot shows the number of cells in each cluster. Cluster 'Undefined 1' was omitted because it only contained 12 cells.* ***e****, Frequency of host and viral gene counts in individual cells.*

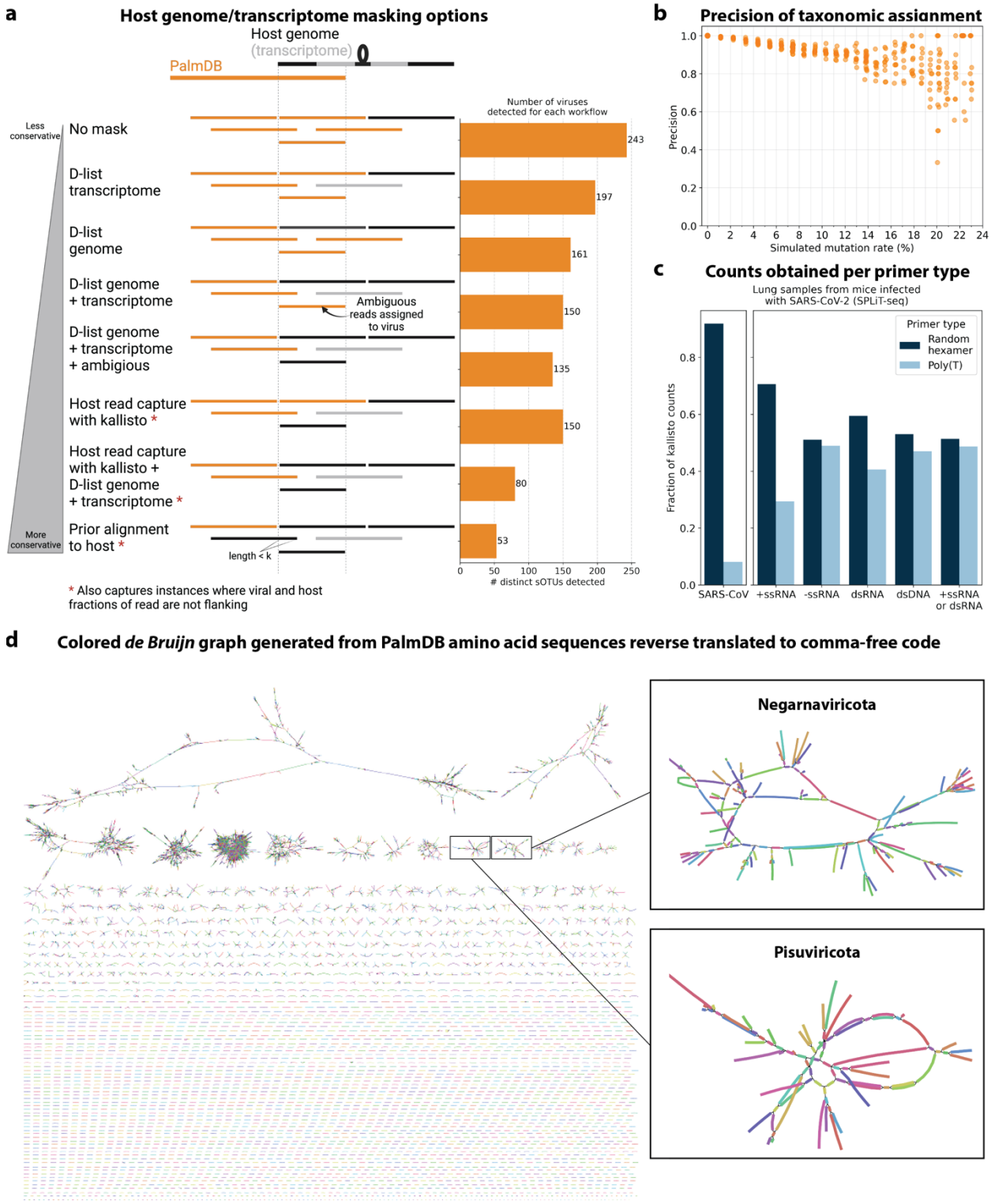

Extended Data Fig. 4: a*, Schematic overview of different host masking options, extending the masking options shown in Fig. 4a. Reads that align to PalmDB and are considered viral are marked in orange, and reads that align to the host genome or transcriptome are marked in black or grey, respectively. The barplot shows the number of distinct sOTUs, defined by distinct virus IDs, observed in ≥ 0.05 % of cells for each workflow.* ***b****, Precision of species-level taxonomic assignment at increasing simulated mutation rates. Mutation-Simulator*[48]

was used to add random single nucleotide base substitutions to 676 ZEBOV *RdRP sequences obtained by Seq-Well sequencing*[37] *at increasing mutation rates. We performed 10 simulations per mutation rate. The sequences were subsequently aligned using kallisto translated search against the complete PalmDB. The recall percentages at each mutation rate are shown in Fig. 2c.* ***c****, Fraction of counts obtained for the known viral infection (here, SARS-CoV-2) and per viral strandedness per primer type. Lung samples from mice infected with SARS-CoV2 were sequenced with SPLiT-Seq*[92] *and aligned to PalmDB using kallisto translated search using the D-list to mask the host (here, mouse) genome. The plot shows the fraction of counts obtained for SARS-CoV as well as all sOTUs of different strandedness per primer type.* ***d****, The de Bruijn graph generated from the reverse translated PalmDB sequences in the kallisto translated search workflow, visualized and colored using Bandage v0.8.1*[93]*.*

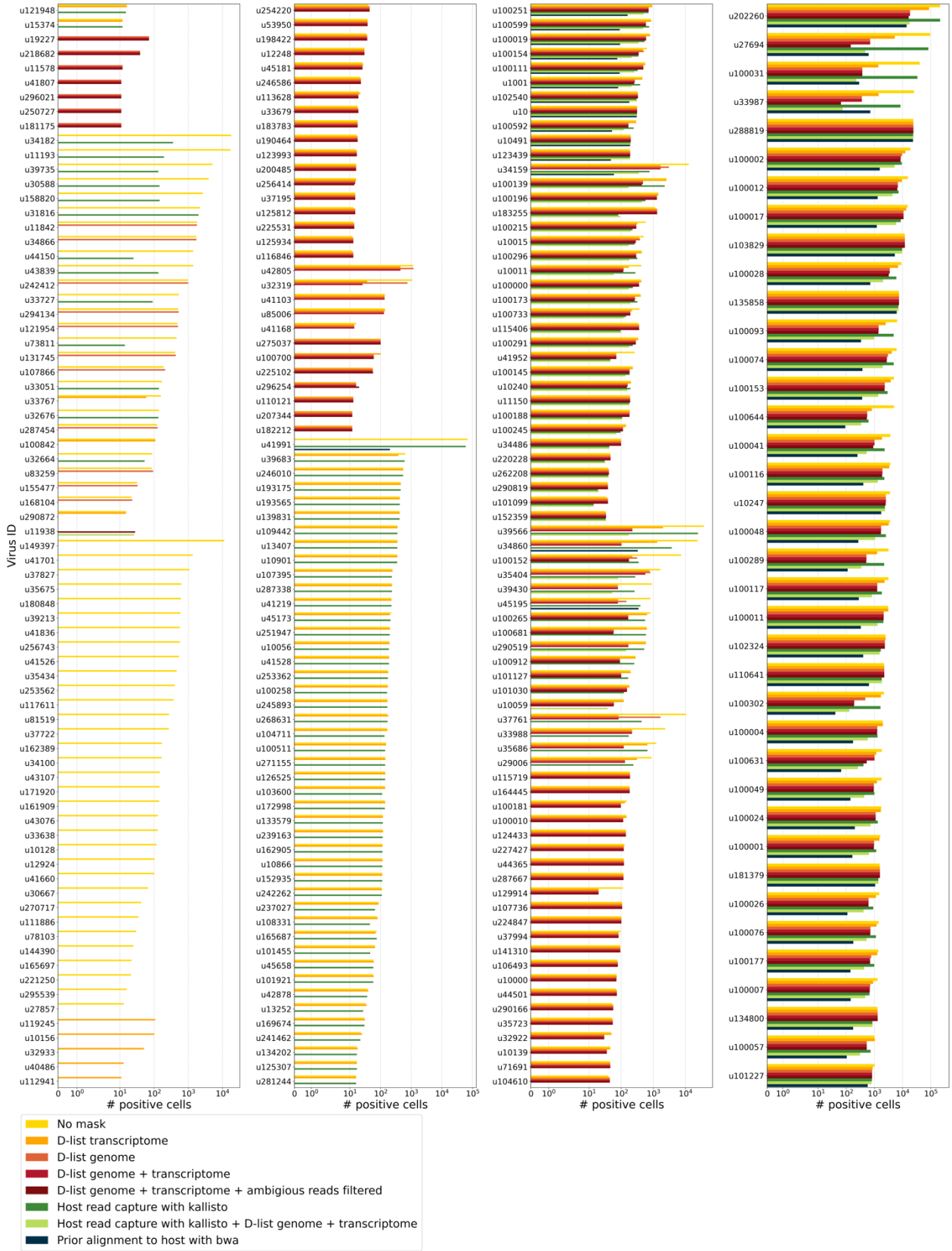

Extended Data Fig. 5: *The number of positive cells for each individual virus ID obtained by different host masking options. Each virus ID shown here was observed in ≥ 0.05 % of cells. The host masking options are visualized in Extended Data Fig. 4a.*

Extended Data Fig. 6: *Number of positive cells per 10k cells for viral species of genera known to infect rhesus macaques[61] in the data from Kotliar et al.[37] analyzed using kallisto translated search with PalmDB. Host sequences were masked using the D-list option with the host genomes and transcriptomes, followed by host read capture using kallisto. No quality control thresholding of viruses was performed. It is notable that we detected Flaviviruses whose genomes are often not polyadenylated, and hence they should not be captured by polyA capture-dependent single-cell RNA sequencing technologies, such as Seq-Well used here. It is possible that these RNA molecules were spuriously captured even though they were not polyadenylated. We also note that the presence of a polyA-tail has been reported for some Flavivirus strains[94].*

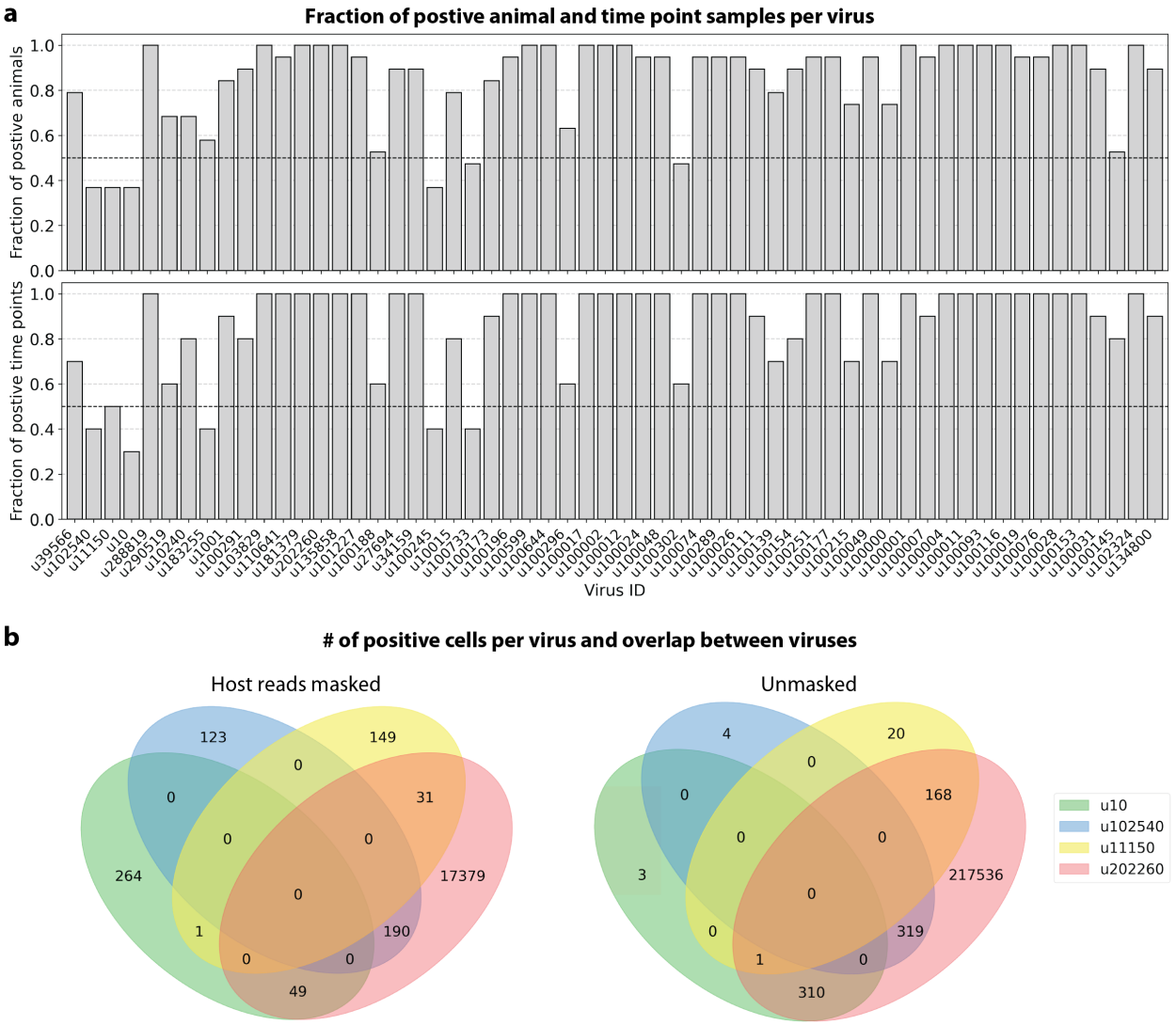

Extended Data Fig. 7: a*, For each virus, the fraction of positive animal (top) and time point (bottom) samples was plotted. A sample was considered positive if at least 0.05 % of cells were positive.* ***b****, The number of positive cells for each virus or any combination of viruses for the count matrices generated from host-masked reads (D-list host genome and transcriptome + host transcriptome read capture) (left) and reads without any host masking (right). A large amount of reads for u202260 were masked when conservatively removing host reads (Fig. 5a). The plots were generated using PyVenn (https://github.com/tctianchi/pyvenn).*

a **Predicting viral presence based on host gene expression**

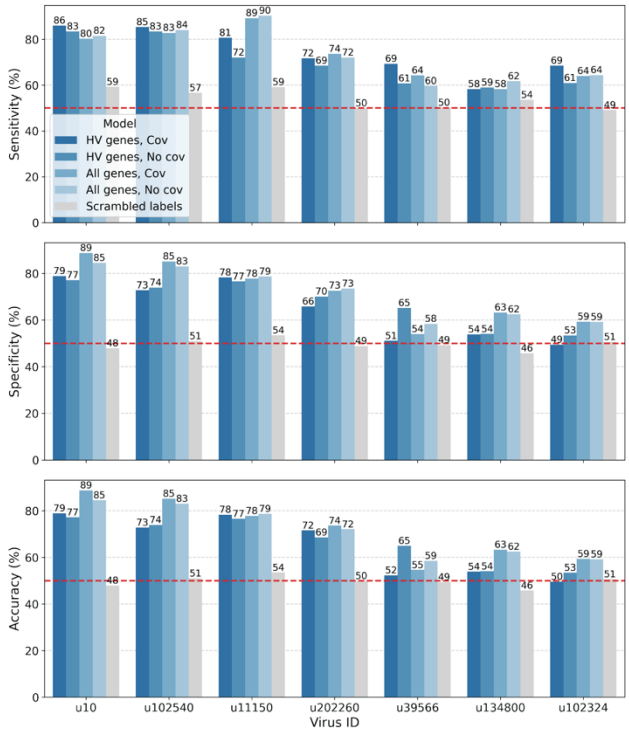

b **Weight correlations of predicitve genes across models**

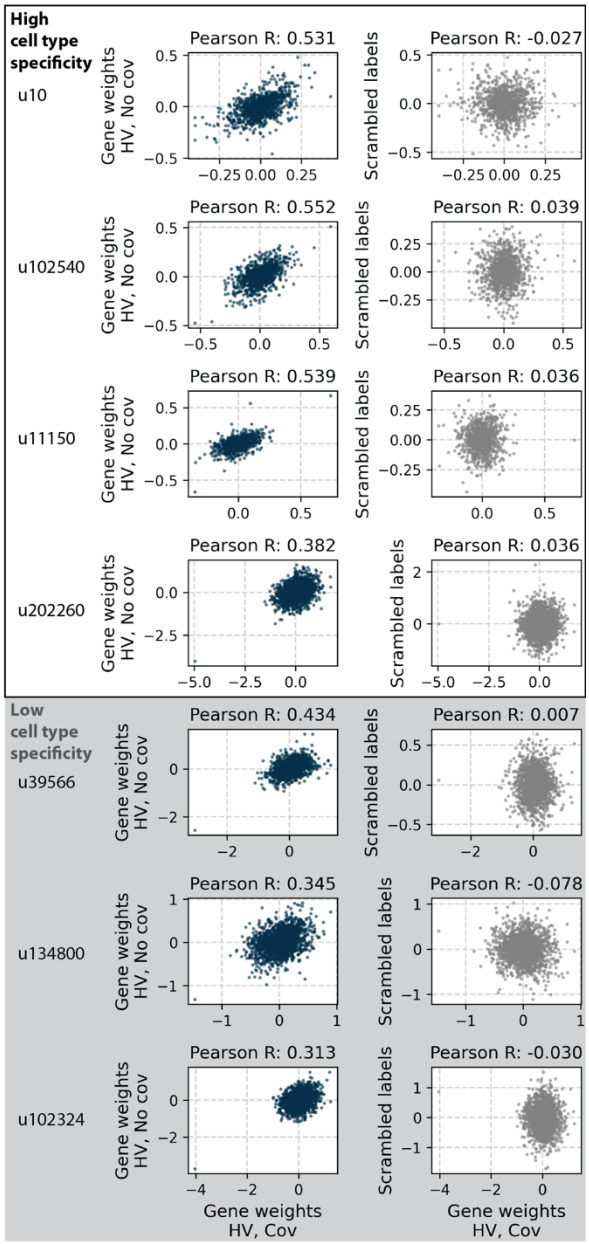

c **# cells used to train and test the logistic regression models**

Virus ID	# training cells	# virus-neg. training cells	# virus-pos. training cells	# testing cells	# virus-neg. testing cells	# virus-pos. testing cells
u10	312	156	156	200,402	200,245	157
u102540	312	156	156	200,402	200,245	157
u11150	186	93	93	200,528	200,435	93
u202260	11,358	5,679	5,679	189,356	5,679	183,677
u39566	21,818	10,909	10,909	178,896	167,987	10,909
u134800	1,148	574	574	199,566	198,991	575
u102324	2,212	1,106	1,106	198,502	197,396	1,106

d **Predicting viral presence based on host gene expression for all shared and 'macaque only' viruses**

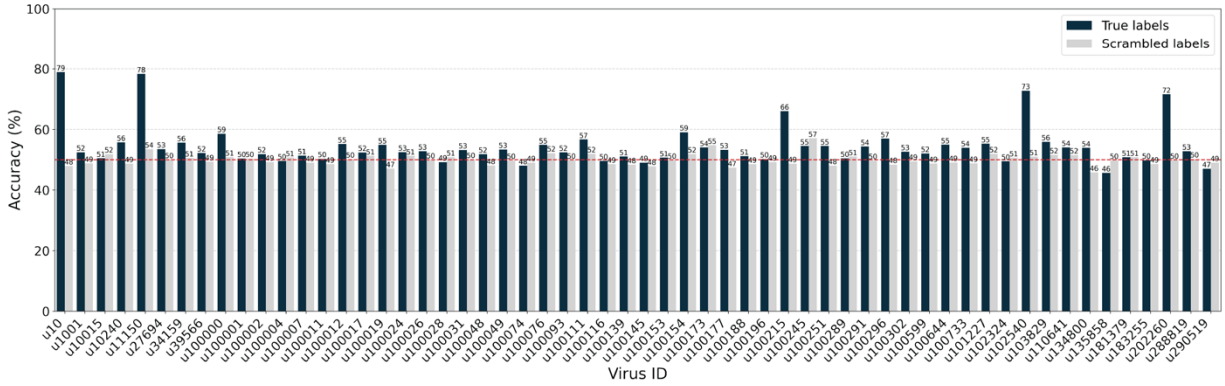

Extended Data Fig. 8: a*, We trained logistic regression models to predict the presence of specific viruses based on host gene expression at single-cell resolution. The accuracy, specificity, and sensitivity of the logistic regression models trained on highly variable (HV) or all macaque genes with or without donor animal and EVD time point as covariates are shown for the known virus ZEBOV (u10) and 6 novel viruses. As a negative control, viral presence and absence labels were scrambled at random in the training data.* ***b****, Weight correlations of the predictive genes for models trained on HV genes with and without covariates on the real and scrambled labels. The weight correlations are lost when the model is trained using the scrambled labels. Viruses with high cell type specificity have slightly higher correlations than viruses with low cell type specificity.* ***c****, The numbers of cells used to train and test the logistic regression models for ZEBOV (u10) and 6 novel viruses.* ***d****, Prediction accuracy of models trained on HV genes with donor animal and EVD time point as covariates for all 'macaque only' and 'shared' viruses.*

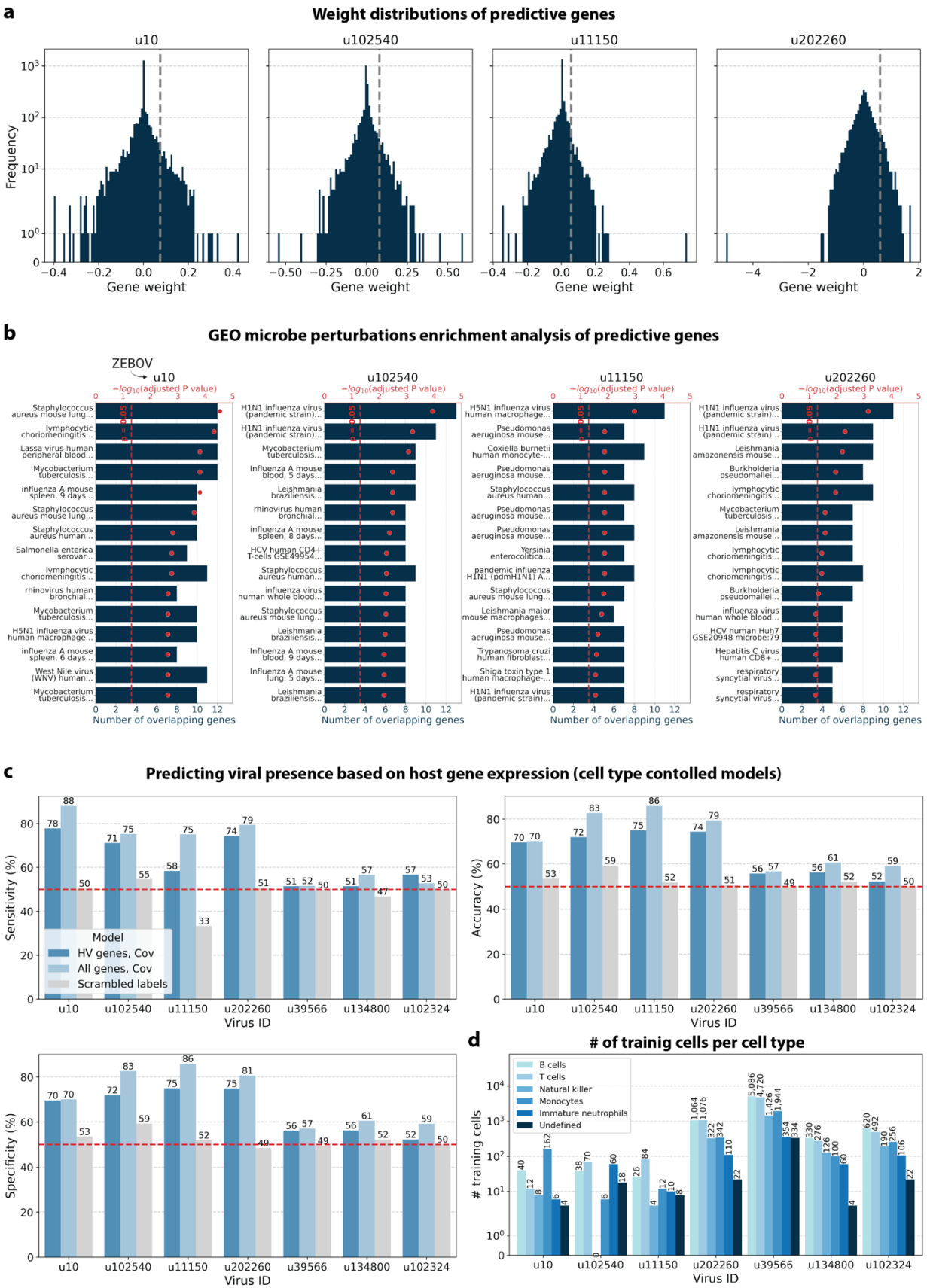
a
Weight distributions of predictive genes
u10
u102540
u11150
u202260
Frequency
Gene weight
b
GEO microbe perturbations enrichment analysis of predictive genes
ZEBOV
u10
u102540
u11150
u202260
−log10(adjusted P value)
Number of overlapping genes
c
Predicting viral presence based on host gene expression (cell type contolled models)
Sensitivity (%)
Accuracy (%)
Specificity (%)
Virus ID
Model
HV genes, Cov
All genes, Cov
Scrambled labels
d
# of trainig cells per cell type
training cells
B cells
T cells
Natural killer
Monocytes
Immature neutrophils
Undefined

Extended Data Fig. 9: a*, Weight distributions of predictive genes from the model trained on highly variable genes with donor and time point as covariates. The dashed, grey line shows the top 200 gene cut-off for the enrichment analysis.* ***b****, Enrichment analysis of the top 200 predictive genes from the model trained on highly variable genes with donor and time point as covariates. Approximately half of the macaque Ensembl IDs did not have annotated gene names, which is a common problem for genomes from non-model organisms. We used gget[45] to translate annotated Ensembl IDs to gene symbols and to perform enrichment analysis using Enrichr[71] against the GEO microbe perturbations database ('Microbe_Perturbations_from_GEO_up')[72]. Reported P values were corrected with the Benjamini-Hochberg method.* ***c****, We performed a second round of modeling whereby virus-negative training cells were selected to be of the same cell types as virus-positive cells. The accuracy, specificity, and sensitivity of these models trained on highly variable (HV) or all macaque genes with donor animal and EVD time point as covariates are shown for the known virus ZEBOV (u10) and 6 novel viruses. As a negative control, viral presence and absence labels were scrambled at random in the training data.* ***d****, Total number of training cells per cell type in the model shown in c. The total consists of an equal number of virus-positive and -negative cells.*

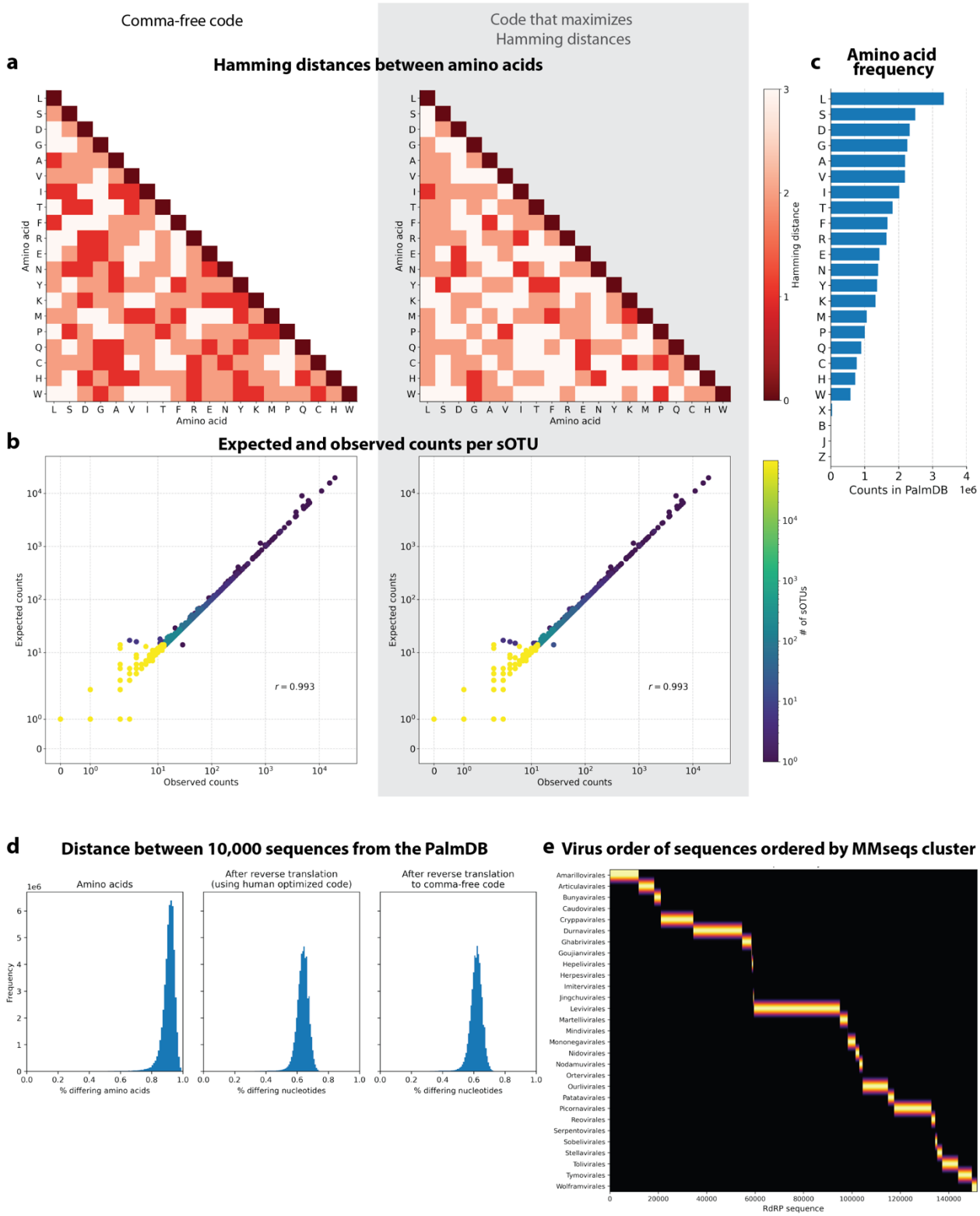

Extended Data Fig. 10: a*, Hamming distances between amino acids in the comma-free code (left) and a second code that maximizes Hamming distances between amino acids that occur most often (right).* ***b****, We reverse translated all amino acid sequences in the PalmDB using the 'standard' genetic code (see Methods). The reverse*

translated PalmDB RdRP sequences were subsequently aligned to the optimized PalmDB amino acid reference (see Methods) with kallisto translated search. The left plot shows the expected and observed counts for each sOTU when kallisto performs the pseudoalignment in the comma-free code space. The plot on the right shows the expected and observed counts for each sOTU when kallisto performs the pseudoalignment using a second code that maximizes the Hamming distances between reverse translated amino acids. ***c****, Occurrence of each amino acid in the PalmDB.* ***d****, Percentage of differing amino acids or nucleotides between 10,000 sequences randomly selected from the PalmDB before and after reverse translation using the standard genetic code (optimized for human) and comma-free code.* ***e****, The virus orders of RdRP sequences sorted based on their clustering by MMseqs2 (see Methods).*

References

1. Mushegian, A. R. Are There 1031 Virus Particles on Earth, or More, or Fewer? *J. Bacteriol.* **202**, (2020).
2. Hendrix, R. W., Hatfull, G. F., Ford, M. E., Smith, M. C. M. & Burns, R. N. Evolutionary relationships among diverse bacteriophages and prophages: all the world's a phage. in *Horizontal gene transfer* 133–VI (Elsevier, 2002).
3. Anthony, S. J. *et al.* A strategy to estimate unknown viral diversity in mammals. *MBio* **4**, e00598–13 (2013).
4. Mollentze, N., Babayan, S. A. & Streicker, D. G. Identifying and prioritizing potential human-infecting viruses from their genome sequences. *PLoS Biol.* **19**, e3001390 (2021).
5. Bjornevik, K. *et al.* Longitudinal analysis reveals high prevalence of Epstein-Barr virus associated with multiple sclerosis. *Science* **375**, 296–301 (2022).
6. Levine, K. S. *et al.* Virus exposure and neurodegenerative disease risk across national biobanks. *Neuron* **111**, 1086–1093.e2 (2023).
7. Cairns, D. M., Itzhaki, R. F. & Kaplan, D. L. Potential Involvement of Varicella Zoster Virus in Alzheimer's Disease via Reactivation of Quiescent Herpes Simplex Virus Type 1. *J. Alzheimers. Dis.* **88**, 1189–1200 (2022).
8. Edgar, R. C. *et al.* Petabase-scale sequence alignment catalyses viral discovery. *Nature* **602**, 142–147 (2022).
9. Leinonen, R., Sugawara, H., Shumway, M. & International Nucleotide Sequence Database Collaboration. The sequence read archive. *Nucleic Acids Res.* **39**, D19–21 (2011).
10. Babaian, A. & Edgar, R. Ribovirus classification by a polymerase barcode sequence. *PeerJ* **10**, e14055 (2022).
11. Chang, J.-T., Liu, L.-B., Wang, P.-G. & An, J. Single-cell RNA sequencing to understand host–virus interactions. *Virol. Sin.* (2023) doi:10.1016/j.virs.2023.11.009.
12. Hill, V. *et al.* Toward a global virus genomic surveillance network. *Cell Host Microbe* **31**, 861–873 (2023).
13. Melsted, P. *et al.* Modular, efficient and constant-memory single-cell RNA-seq preprocessing. *Nat. Biotechnol.* **39**, 813–818 (2021).
14. Ren, J. *et al.* Identifying viruses from metagenomic data using deep learning. *Quant Biol* **8**, 64–77 (2020).
15. Tithi, S. S., Aylward, F. O., Jensen, R. V. & Zhang, L. FastViromeExplorer: a pipeline for virus and phage identification and abundance profiling in metagenomics data. *PeerJ* **6**, e4227 (2018).
16. Camargo, A. P. *et al.* You can move, but you can't hide: identification of mobile genetic elements with geNomad. *bioRxiv* (2023) doi:10.1101/2023.03.05.531206.
17. Amgarten, D., Braga, L. P. P., da Silva, A. M. & Setubal, J. C. MARVEL, a Tool for Prediction of Bacteriophage Sequences in Metagenomic Bins. *Front. Genet.* **9**, 304 (2018).
18. Starikova, E. V. *et al.* Phigaro: high-throughput prophage sequence annotation. *Bioinformatics* **36**, 3882–3884 (2020).
19. Kieft, K., Zhou, Z. & Anantharaman, K. VIBRANT: automated recovery, annotation and curation of microbial viruses, and evaluation of viral community function from genomic sequences. *Microbiome* **8**, 90 (2020).
20. Antipov, D., Raiko, M., Lapidus, A. & Pevzner, P. A. Metaviral SPAdes: assembly of viruses from

metagenomic data. *Bioinformatics* **36**, 4126–4129 (2020).
21. Ren, J., Ahlgren, N. A., Lu, Y. Y., Fuhrman, J. A. & Sun, F. VirFinder: a novel k-mer based tool for identifying viral sequences from assembled metagenomic data. *Microbiome* **5**, 69 (2017).
22. Guo, J. *et al.* VirSorter2: a multi-classifier, expert-guided approach to detect diverse DNA and RNA viruses. *Microbiome* **9**, 37 (2021).
23. Xia, Y., Liu, Y., Deng, M. & Xi, R. Detecting virus integration sites based on multiple related sequencing data by VirTect. *BMC Med. Genomics* **12**, 19 (2019).
24. Bost, P. *et al.* Host-Viral Infection Maps Reveal Signatures of Severe COVID-19 Patients. *Cell* **181**, 1475–1488.e12 (2020).
25. Lee, C. Y. *et al.* Venus: An efficient virus infection detection and fusion site discovery method using single-cell and bulk RNA-seq data. *PLoS Comput. Biol.* **18**, e1010636 (2022).
26. Yasumizu, Y., Hara, A., Sakaguchi, S. & Ohkura, N. VIRTUS: a pipeline for comprehensive virus analysis from conventional RNA-seq data. *Bioinformatics* **37**, 1465–1467 (2021).
27. Wood, D. E., Lu, J. & Langmead, B. Improved metagenomic analysis with Kraken 2. *Genome Biol.* **20**, 257 (2019).
28. Buchfink, B., Reuter, K. & Drost, H.-G. Sensitive protein alignments at tree-of-life scale using DIAMOND. *Nat. Methods* **18**, 366–368 (2021).
29. Golomb, S. W., Gordon, B. & Welch, L. R. Comma-Free Codes. *Canad. J. Math.* **10**, 202–209 (1958).
30. Crick, F. H., Griffith, J. S. & Orgel, L. E. CODES WITHOUT COMMAS. *Proc. Natl. Acad. Sci. U. S. A.* **43**, 416–421 (1957).
31. Macosko, E. Z. *et al.* Highly Parallel Genome-wide Expression Profiling of Individual Cells Using Nanoliter Droplets. *Cell* **161**, 1202–1214 (2015).
32. Ramsköld, D. *et al.* Full-length mRNA-Seq from single-cell levels of RNA and individual circulating tumor cells. *Nat. Biotechnol.* **30**, 777–782 (2012).
33. Rosenberg, A. B. *et al.* Single-cell profiling of the developing mouse brain and spinal cord with split-pool barcoding. *Science* **360**, 176–182 (2018).
34. Desai, N. *et al.* Temporal and spatial heterogeneity of host response to SARS-CoV-2 pulmonary infection. *Nat. Commun.* **11**, 6319 (2020).
35. Viloria Winnett, A. *et al.* Morning SARS-CoV-2 Testing Yields Better Detection of Infection Due to Higher Viral Loads in Saliva and Nasal Swabs upon Waking. *Microbiol Spectr* **10**, e0387322 (2022).
36. Viloria Winnett, A. *et al.* Extreme differences in SARS-CoV-2 viral loads among respiratory specimen types during presumed pre-infectious and infectious periods. *PNAS Nexus* **2**, gad033 (2023).
37. Kotliar, D. *et al.* Single-Cell Profiling of Ebola Virus Disease In Vivo Reveals Viral and Host Dynamics. *Cell* **183**, 1383–1401.e19 (2020).
38. Sharma, A. *et al.* Human iPSC-Derived Cardiomyocytes Are Susceptible to SARS-CoV-2 Infection. *Cell Rep Med* **1**, 100052 (2020).
39. Langmead, B. & Salzberg, S. L. Fast gapped-read alignment with Bowtie 2. *Nat. Methods* **9**, 357–359 (2012).
40. Danecek, P. *et al.* Twelve years of SAMtools and BCFtools. *Gigascience* **10**, (2021).
41. Kuznetsov, A. & Bollin, C. J. NCBI Genome Workbench: Desktop Software for Comparative Genomics, Visualization, and GenBank Data Submission. *Methods Mol. Biol.* **2231**, 261–295 (2021).
42. Peck, K. M. & Lauring, A. S. Complexities of Viral Mutation Rates. *J. Virol.* **92**, (2018).
43. Sullivan, D. K. *et al.* kallisto, bustools, and kb-python for quantifying bulk, single-cell, and single-nucleus RNA-seq. *bioRxiv* 2023.11.21.568164 (2023) doi:10.1101/2023.11.21.568164.

44. Melsted, P. *et al.* Modular and efficient pre-processing of single-cell RNA-seq. *bioRxiv* 673285 (2019) doi:10.1101/673285.
45. Luebbert, L. & Pachter, L. Efficient querying of genomic reference databases with gget. *Bioinformatics* **39**, (2023).
46. Letunic, I. & Bork, P. Interactive Tree Of Life (iTOL) v5: an online tool for phylogenetic tree display and annotation. *Nucleic Acids Res.* **49**, W293–W296 (2021).
47. Lu, J. & Salzberg, S. L. Ultrafast and accurate 16S rRNA microbial community analysis using Kraken 2. *Microbiome* **8**, 124 (2020).
48. Kühl, M. A., Stich, B. & Ries, D. C. Mutation-Simulator: fine-grained simulation of random mutations in any genome. *Bioinformatics* **37**, 568–569 (2021).
49. Gihawi, A. *et al.* Major data analysis errors invalidate cancer microbiome findings. *MBio* e0160723 (2023).
50. Breitwieser, F. P., Pertea, M., Zimin, A. V. & Salzberg, S. L. Human contamination in bacterial genomes has created thousands of spurious proteins. *Genome Res.* **29**, 954–960 (2019).
51. Steinegger, M. & Salzberg, S. L. Terminating contamination: large-scale search identifies more than 2,000,000 contaminated entries in GenBank. *Genome Biol.* **21**, 115 (2020).
52. Wang, J. & Han, G.-Z. Genome mining shows that retroviruses are pervasively invading vertebrate genomes. *Nat. Commun.* **14**, 4968 (2023).
53. Hjörleifsson, K. E., Sullivan, D. K., Holley, G., Melsted, P. & Pachter, L. Accurate quantification of single-nucleus and single-cell RNA-seq transcripts. *bioRxiv* 2022.12.02.518832 (2022) doi:10.1101/2022.12.02.518832.
54. Li, H. Aligning sequence reads, clone sequences and assembly contigs with BWA-MEM. *arXiv [q-bio.GN]* (2013).
55. Altschul, S. F., Gish, W., Miller, W., Myers, E. W. & Lipman, D. J. Basic local alignment search tool. *J. Mol. Biol.* **215**, 403–410 (1990).
56. Camacho, C. *et al.* BLAST+: architecture and applications. *BMC Bioinformatics* **10**, 421 (2009).
57. Warren, W. C. *et al.* Sequence diversity analyses of an improved rhesus macaque genome enhance its biomedical utility. *Science* **370**, (2020).
58. Traag, V. A., Waltman, L. & van Eck, N. J. From Louvain to Leiden: guaranteeing well-connected communities. *Sci. Rep.* **9**, 5233 (2019).
59. Svensson, V., da Veiga Beltrame, E. & Pachter, L. Quantifying the tradeoff between sequencing depth and cell number in single-cell RNA-seq. *bioRxiv* 762773 (2019) doi:10.1101/762773.
60. Feldmann, H. & Geisbert, T. W. Ebola haemorrhagic fever. *Lancet* **377**, 849–862 (2011).
61. Wachtman, L. & Mansfield, K. Chapter 1 - Viral Diseases of Nonhuman Primates. in *Nonhuman Primates in Biomedical Research (Second Edition)* (eds. Abee, C. R., Mansfield, K., Tardif, S. & Morris, T.) 1–104 (Academic Press, 2012).
62. Ondov, B. D., Bergman, N. H. & Phillippy, A. M. Interactive metagenomic visualization in a Web browser. *BMC Bioinformatics* **12**, 385 (2011).
63. Porter, A. F., Cobbin, J., Li, C.-X., Eden, J.-S. & Holmes, E. C. Metagenomic Identification of Viral Sequences in Laboratory Reagents. *Viruses* **13**, (2021).
64. Blomberg, J. *et al.* Phylogeny-directed search for murine leukemia virus-like retroviruses in vertebrate genomes and in patients suffering from myalgic encephalomyelitis/chronic fatigue syndrome and prostate cancer. *Adv. Virol.* **2011**, 341294 (2011).
65. Callanan, J. *et al. Rename one class (Leviviricetes - formerly Allassoviricetes), rename one order*

(Norzivirales - formerly Levivirales), create one new order (Timlovirales), and expand the class to a total of six families, 420 genera and 883 species. http://rgdoi.net/10.13140/RG.2.2.25363.40481 (2021) doi:10.13140/RG.2.2.25363.40481.
66. Callanan, J. *et al.* Expansion of known ssRNA phage genomes: From tens to over a thousand. *Sci Adv* **6**, eaay5981 (2020).
67. Cohen, J. I. Herpesvirus latency. *J. Clin. Invest.* **130**, 3361–3369 (2020).
68. Woźniakowski, G. & Samorek-Salamonowicz, E. Animal herpesviruses and their zoonotic potential for cross-species infection. *Ann. Agric. Environ. Med.* **22**, 191–194 (2015).
69. Yao, X. *et al.* In Vitro Infection Dynamics of Wuxiang Virus in Different Cell Lines. *Viruses* **14**, (2022).
70. Valles, S. M. *et al.* ICTV Virus Taxonomy Profile: Iflaviridae. *J. Gen. Virol.* **98**, 527–528 (2017).
71. Kuleshov, M. V. *et al.* Enrichr: a comprehensive gene set enrichment analysis web server 2016 update. *Nucleic Acids Res.* **44**, W90–7 (2016).
72. Kanehisa, M., Furumichi, M., Sato, Y., Kawashima, M. & Ishiguro-Watanabe, M. KEGG for taxonomy-based analysis of pathways and genomes. *Nucleic Acids Res.* **51**, D587–D592 (2023).
73. Tomlin, H. & Piccinini, A. M. A complex interplay between the extracellular matrix and the innate immune response to microbial pathogens. *Immunology* **155**, 186–201 (2018).
74. Saxena, M. & Yeretssian, G. NOD-Like Receptors: Master Regulators of Inflammation and Cancer. *Front. Immunol.* **5**, 327 (2014).
75. Zenobia, C. & Hajishengallis, G. Basic biology and role of interleukin-17 in immunity and inflammation. *Periodontol. 2000* **69**, 142–159 (2015).
76. Bonjardim, C. A., Ferreira, P. C. P. & Kroon, E. G. Interferons: signaling, antiviral and viral evasion. *Immunol. Lett.* **122**, 1–11 (2009).
77. Layrolle, P., Payoux, P. & Chavanas, S. PPAR Gamma and Viral Infections of the Brain. *Int. J. Mol. Sci.* **22**, (2021).
78. Cheema, P. S., Nandi, D. & Nag, A. Exploring the therapeutic potential of forkhead box O for outfoxing COVID-19. *Open Biol.* **11**, 210069 (2021).
79. Nailwal, H. & Chan, F. K.-M. Necroptosis in anti-viral inflammation. *Cell Death Differ.* **26**, 4–13 (2019).
80. Blanch-Ruiz, M. A., Ortega-Luna, R., Gómez-García, G., Martínez-Cuesta, M. Á. & Álvarez, Á. Role of Neutrophil Extracellular Traps in COVID-19 Progression: An Insight for Effective Treatment. *Biomedicines* **10**, (2021).
81. Huber, V. C., Lynch, J. M., Bucher, D. J., Le, J. & Metzger, D. W. Fc receptor-mediated phagocytosis makes a significant contribution to clearance of influenza virus infections. *J. Immunol.* **166**, 7381–7388 (2001).
82. Gierahn, T. M. *et al.* Seq-Well: portable, low-cost RNA sequencing of single cells at high throughput. *Nat. Methods* **14**, 395–398 (2017).
83. Hughes, T. K. *et al.* Second-Strand Synthesis-Based Massively Parallel scRNA-Seq Reveals Cellular States and Molecular Features of Human Inflammatory Skin Pathologies. *Immunity* **53**, 878–894.e7 (2020).
84. Melsted, P., Ntranos, V. & Pachter, L. The barcode, UMI, set format and BUStools. *Bioinformatics* **35**, 4472–4473 (2019).
85. Pirtskhalava, M. *et al.* DBAASP v3: database of antimicrobial/cytotoxic activity and structure of peptides as a resource for development of new therapeutics. *Nucleic Acids Res.* **49**, D288–D297

(2021).
86. Abdill, R. J. *et al.* Integration of 168,000 samples reveals global patterns of the human gut microbiome. *bioRxiv* (2023) doi:10.1101/2023.10.11.560955.
87. Hauser, M., Steinegger, M. & Söding, J. MMseqs software suite for fast and deep clustering and searching of large protein sequence sets. *Bioinformatics* **32**, 1323–1330 (2016).
88. Lu, J. *et al.* Metagenome analysis using the Kraken software suite. *Nat. Protoc.* **17**, 2815–2839 (2022).
89. Cock, P. J. A. *et al.* Biopython: freely available Python tools for computational molecular biology and bioinformatics. *Bioinformatics* **25**, 1422–1423 (2009).
90. Zulkower, V. & Rosser, S. DNA Chisel, a versatile sequence optimizer. *Bioinformatics* **36**, 4508–4509 (2020).
91. Wolf, F. A., Angerer, P. & Theis, F. J. SCANPY: large-scale single-cell gene expression data analysis. *Genome Biol.* **19**, 15 (2018).
92. Ostendorf, B. N. *et al.* Common human genetic variants of APOE impact murine COVID-19 mortality. *Nature* **611**, 346–351 (2022).
93. Wick, R. R., Schultz, M. B., Zobel, J. & Holt, K. E. Bandage: interactive visualization of de novo genome assemblies. *Bioinformatics* **31**, 3350–3352 (2015).
94. Mandl C W, Kunz C & Heinz F X. Presence of poly(A) in a flavivirus: significant differences between the 3' noncoding regions of the genomic RNAs of tick-borne encephalitis virus strains. *J. Virol.* **65**, 4070–4077 (1991).